

Charge transfer transitions and circular magneto-optics in ferrites

A.S. Moskvina

Ural Federal University, 620083 Ekaterinburg, Russia and

M.N. Mikheev Institute of Metal Physics of Ural Branch of Russian Academy of Sciences, 620108 Ekaterinburg, Russia

The concept of charge-transfer (CT) transitions in ferrites is based on the cluster approach and takes into account the relevant interactions as the low-symmetry crystal field, spin-orbital, Zeeman, exchange and exchange-relativistic interactions. For all its simplicity, this concept yields a reliable qualitative and quantitative microscopic explanation of spectral, concentration, temperature, and field dependences of optic and magneto-optic properties ranging from the isotropic absorption as well as the optic anisotropy to the circular magneto-optics. In this review paper, starting with a critical analysis of the fundamental shortcomings of the "first-principles" DFT-based band theory we present the main ideas and techniques of the cluster theory of the CT transitions to be main contributors to circular magneto-optics of ferrites.

I. INTRODUCTION

Over the past 175 years since Michael Faraday's discovery of the relation between light and electromagnetism, magneto-optics has become a broad field of fundamental and applied research. On the one hand, magneto-optics is aimed at the experimental study of the electronic and magnetic structure, magnetic anisotropy, magnetic phase transitions, spin-orbital, exchange and exchange-relativistic effects, and on the other hand, at the search for new materials with high magneto-optical characteristics, improvement and development of new magneto-optical applications. Various ferrites and, especially, bismuth-substituted iron garnets $R_3Fe_5O_{12}$ ($R = Y$, or rare-earth ion) occupy a special place among magneto-optical (MO) materials, being one of the main objects of fundamental research and basic materials for creating various devices of applied magneto-optics from magneto-optical sensors and visualizers, the terahertz isolators, circulators, magneto-optical modulators, optical magnetoelectric sensors, nonreciprocal elements of the integrated optics, to promising applications in high density MO data-storage and low-power consumption spintronic nanodevices.

Rare-earth orthoferrites $RFeO_3$, which have been studied since the 60s of the last century, have attracted and continue to attract the particular attention of researchers for several decades owing to their weak ferromagnetism, remarkable magneto-optical properties, spin-reorientation transitions between antiferromagnetic phases, high velocity of domain walls, and many other properties. Their physical properties remain a focus of considerable research due to promising applications in innovative spintronic devices, furthermore, they contribute to an emerging class of materials, multiferroics with strong magnetoelectric coupling.

The problem of describing the optical and magneto-optical properties of ferrites is one of the most challenging tasks in the theory of strongly correlated 3d compounds. Despite many years of experimental and theoretical research, the nature of their optical and, especially, magneto-optical response remains a subject of de-

bate. This concerns both the identification of electronic transitions responsible for the formation of the main optical and magneto-optical properties and the comprehensive calculation of their contribution to the optical and magneto-optical response functions. The solution of this problem largely depends on the choice of the optimal strategy for taking into account the effects of charge transfer and strong local correlations, which can be formulated as the choice of a compromise between the one-electron band and atomic-molecular description of electronic states.

The nature of the low-energy optical electron-hole excitations in the insulating transition metal 3d oxides represents one of the most important challenging issues for these strongly correlated systems. All these excitations are especially interesting because they could play a central role in multiband Hubbard models used to describe both the insulating state and the unconventional states developed under electron or hole doping. Because of the matrix element effect the optical response does provide only an indirect information about the density of states. Nevertheless it remains one of the most efficient techniques to inspect the electronic structure and energy spectrum.

In this review paper, we present a critical analysis of band approaches to describing the optical and magneto-optical response of 3d ferrite-type compounds based on the use of density functional theory (DFT) and argue that the traditional physically transparent atomic-molecular cluster approach (see, e.g., [1-3] and references therein) based on local symmetry, strong covalence and charge transfer (CT) effects with strong local correlations, provides a consistent description and explanation of the optical and magneto-optical response of various ferrites in a wide spectral range. The review was stimulated by the lack of detailed and reliable studies of electron-hole excitations and of a proper understanding of the relative role of different transitions to optical and magneto-optical response for ferrites.

The rest of the paper is organized as follows. In Sec. 2 we present a critical overview of the DFT based approaches for description of the optical and magneto-optical properties of strongly correlated 3d compounds and

point to the cluster model as a comprehensive physically clear alternative to the DFT approach. In Sec. 3 we address the charge transfer (CT) states and CT transitions in octahedral $[\text{FeO}_6]^{9-}$ and tetrahedral $[\text{FeO}_4]^{5-}$ clusters as basic elements of crystalline and electronic structure for most ferrites. Here we also show that the CT transitions provide an adequate description of the optical spectra for a wide range of ferrites and other 3d oxides. In Sec. 4 we discuss different interactions for the CT states with a specific focus on so-called exchange-relativistic interactions, in particular, novel "spin-other-orbit" interaction. In Sec. 5 we analyze the polarisability tensor for the octahedral $[\text{FeO}_6]^{9-}$ cluster and argue that its contribution to the optical and magneto-optical anisotropy is determined by different interactions in excited states. In Sec. 6 we overview different points of a microscopic theory of circular magneto-optics for ferrite-garnets and weak ferromagnets, including Bi-substituted garnets, specific role of the "spin-other-orbit" coupling in weak ferromagnetic ferrites, the temperature dependence of circular magneto-optics, and the role of the 4f-5d transitions in rare-earth ions. A brief summary is given in Sec. 7.

II. DENSITY FUNCTIONAL THEORY OR CLUSTER MODEL?

A. So-called "ab initio" DFT based approaches

The electronic states in strongly correlated 3d oxides manifest both significant localization and dispersive features. One strategy to deal with this dilemma is to restrict oneself to small many-electron clusters embedded to a whole crystal, then creating model effective lattice Hamiltonians whose spectra may reasonably well represent the energy and dispersion of the important excitations of the full problem. Despite some shortcomings the method did provide a clear physical picture of the complex electronic structure and the energy spectrum, as well as the possibility of a quantitative modeling.

However, last decades the condensed matter community faced an expanding flurry of papers with the so called *ab initio* calculations of electronic structure and physical properties for strongly correlated systems such as 3d compounds based on density functional theory [4, 5]. Only in recent years has a series of papers been published on *ab initio* calculations of the electronic structure, optical and magneto-optical spectra of iron garnets (see e.g., Refs. [6–8]).

However, DFT still remains, in some sense, ill-defined: many of DFT statements were ill-posed or not rigorously proved. All efforts to account for the correlations beyond LDA (local density approximation) encounter an insoluble problem of double counting (DC) of interaction terms which had just included into Kohn-Sham single-particle potential.

Most widely used DFT computational schemes start with a "metallic-like" approaches making use of approx-

imate energy functionals, firstly LDA scheme, which are constructed as expansions around the homogeneous electron gas limit and fail quite dramatically in capturing the properties of strongly correlated systems. The LDA+U and LDA+DMFT (DMFT, dynamical mean-field theory) [9] methods are believed to correct the inaccuracies of approximate DFT exchange correlation functionals. The main idea of these computational approaches consists in a selective description of the strongly correlated electronic states, typically, localized *d* or *f* orbitals, using the Hubbard model, while all the other states continue to be treated at the level of standard approximate DFT functionals. At present the LDA+U and LDA+DMFT methods are addressed to be most powerful tools for the investigation of strongly correlated electronic systems, however, these preserve many shortcomings of the DFT-LDA approach.

Usually the values of effective on-site Coulomb parameters $U_{eff} = U - J$, where U represent the *ad hoc* Hubbard on-site Coulomb repulsion parameter and J the intra-atomic Hund's exchange integral, are ordinarily determined by seeking a good agreement of the calculated properties with the experimental results such as band gaps or oxidation energies. The values of U_{eff} affect strongly the calculated material properties even in the ground state, so that it is desirable to find its optimal values, which also depend on the chosen exchange-correlation functional. Recent studies have attempted to calculate these parameters directly based on first principles approaches. Nevertheless, the calculated values differ widely, even for the same ionic state in a given material, due to a number of factors such as the choice of the DFT scheme or the underlying basis set. Although it has become a common practice that a certain U_{eff} value is chosen *a priori* during the setup of a first principles-based calculation, it is also well known that a certain U_{eff} value may not work definitively for all calculation methods and DFT schemes. By independently constraining the field on the Fe atoms at the octahedral and tetrahedral sites in YIG, the authors [8] have obtained two different values of U_{eff} , i.e., 9.8 eV for octa-Fe and 9.1 eV for tetra-Fe. These values are considerably different from those used for iron garnets in previous works, e.g. $U = 3.5$ eV and $J = 0.8$ eV [10] using the orthonormalized linear combination of atomic orbitals basis set within constrained LDA approach and $U_{eff} = 5.7$ eV [11], $U = 4$ eV [7, 12]. The Hubbard and Hund's U and J parameters were chosen as $U_{eff} = 2.7$ eV for YIG, 4.7 eV for LuIG, and 5 eV for Bi-substituted garnet $\text{Bi}_x\text{Lu}_{3-x}\text{Fe}_5\text{O}_{12}$ [13].

Despite many examples of a seemingly good agreement with experimental data (photoemission and inverse-photoemission spectra, magnetic moments,...) claimed by the DFT community, both the questionable starting point and many unsolved and unsolvable problems give rise to serious doubts in quantitative and even qualitative predictions made within the DFT based techniques.

Strictly speaking, the DFT is designed for description of ground rather than excited states with no good scheme

for excitations. Because an excited-state density does not uniquely determine the potential, there is no general analog of the Hohenberg-Kohn functional for excited states. The standard functionals are inaccurate both for on-site crystal field and for charge transfer excitations [14]. The DFT based approaches cannot provide the correct atomic limit and the term and multiplet structure [15, 16], which is crucial for description of the optical response for 3d compounds. Although there are efforts to obtain correct results for spectroscopic properties depending on spin and orbital density this problem remains as an open one in DFT research. Clearly, all these difficulties stem from unsolved foundational problems in DFT and are related to fractional charges and to fractional spins. Thus, these basic unsolved issues in the DFT point toward the need for a basic understanding of foundational issues.

In other words, given these background problems, the DFT based models should be addressed as semi-empirical approximate ones rather than *ab initio* theories. M. Levy introduced in 2010 the term DFA to define density functional approximation instead of DFT, which is believed to quite appropriately describe contemporary DFT [17].

Basic drawback of the spin-polarized approaches to description of electronic structure for spin-magnetic systems, especially in a simple LSDA scheme [6], is that these start with a local density functional in the form

$$\mathbf{v}(\mathbf{r}) = v_0[n(\mathbf{r})] + \Delta v[n(\mathbf{r}), \mathbf{m}(\mathbf{r})](\hat{\boldsymbol{\sigma}} \cdot \frac{\mathbf{m}(\mathbf{r})}{|\mathbf{m}(\mathbf{r})|}),$$

where $n(\mathbf{r})$, $\mathbf{m}(\mathbf{r})$ are the electron and spin magnetic density, respectively, $\hat{\boldsymbol{\sigma}}$ is the Pauli matrix, that is these imply presence of a large fictitious local *one-electron* spin-magnetic field $\propto (v^\uparrow - v^\downarrow)$, where $v^{\uparrow,\downarrow}$ are the on-site LSDA spin-up and spin-down potentials. Magnitude of the field is considered to be governed by the intra-atomic Hund exchange, while its orientation does by the effective molecular, or inter-atomic exchange fields. Despite the supposedly spin nature of the field it produces an unphysically giant spin-dependent rearrangement of the charge density that cannot be reproduced within any conventional technique operating with spin Hamiltonians. Furthermore, a direct link with the orientation of the field makes the effect of the spin configuration onto the charge distribution to be unphysically large. However, magnetic long-range order has no significant influence on the redistribution of the charge density. In such a case the straightforward application of the LSDA scheme can lead to an unphysical overestimation of the effects or even to qualitatively incorrect results due to an unphysical effect of a breaking of spatial symmetry induced by a spin configuration. The DFT-LSDA community needed many years to understand such a physically clear point.

Overall, the LSDA approach seems to be more or less justified for a semi-quantitative description of exchange coupling effects for materials with a classical Néel-like collinear magnetic order. However, it can lead to erroneous results for systems and high-order perturbation effects where the symmetry breaking and quantum fluc-

tuations are of a principal importance such as: i) non-collinear spin configurations, in particular, in quantum $s = 1/2$ magnets; ii) relativistic effects, such as the symmetric spin anisotropy, antisymmetric DM coupling; iii) spin-dependent electric polarization; iv) circular magneto-optical effects.

In general, the LSDA method to handle a spin degree of freedom is absolutely incompatible with a conventional approach based on the spin Hamiltonian concept. There are some intractable problems with a match making between the conventional formalism of a spin Hamiltonian and LSDA approach to the exchange and exchange-relativistic effects. Visibly plausible numerical results for different exchange and exchange-relativistic parameters reported in many LSDA investigations (see, e.g., Refs. [18]) evidence only a potential capacity of the LSDA based models for semiquantitative estimations, rather than for reliable quantitative data.

It is rather surprising how little attention has been paid to the DFT based calculations of the optical properties for the transition metal oxides (TMO). Lets turn to a recent paper by Roedel and Bechstedt [19] on NiO and other TMOs, whose approach is typical for DFT community. The authors calculated the dielectric function $\epsilon(\omega)$ for NiO within the DFT-GGA+U+ Δ technique and claim: "The experimental data agree very well with the calculated curves" (!?). However, this seeming agreement is a result of a simple fitting when the two model parameters U and Δ are determined such ($U = 3.0$, $\Delta = 2.0$ eV) that the best possible agreement concerning the positions and intensities of the characteristic peaks in the experimental spectra is obtained. In addition, the authors arrive at absolutely unphysical conclusion: "The optical absorption of NiO is dominated by intra-atomic $t_{2g} \rightarrow e_g$ transitions" (!?).

There are still a lot of people who think the Hohenberg-Kohn-Sham DFT within the LDA has provided a very successful *ab initio* framework to successfully tackle the problem of the electronic structure of materials. However, both the starting point and realizations of the DFT approach have raised serious questions. The HK "theorem" of the existence of a mythical universal density functional that can resolve everything looks like a way into Neverland, the DFT heaven is probably unattainable. Various DFAs, density functional approximations, local or nonlocal, will never be exact. Users are willing to pay this price for simplicity, efficacy, and speed, combined with useful (but not yet chemical or physical) accuracy [14, 20].

The most popular DFA fail for the most interesting systems, such as strongly correlated oxides, in particular ferrites. The standard DFT approximations over-delocalize the 3d-electrons, leading to highly incorrect descriptions. Some practical schemes, in particular, DMFT can correct some of these difficulties, but none has yet become a universal tool of known performance for such systems [14].

B. Cluster model approach

At variance with the DFT theory the cluster model approach does generalize and advance crystal-field and ligand-field theory. The method provides a clear physical picture of the complex electronic structure and the energy spectrum, as well as the possibility of a quantitative modeling. In a certain sense the cluster calculations might provide a better description of the overall electronic structure of insulating 3d oxides than the band structure calculations [21, 22], mainly due to a better account for correlation effects, electron-lattice coupling, and relatively weak interactions such as spin-orbital and exchange coupling. Moreover, the cluster model has virtually no competitors in the description of impurity or dilute systems. Cluster models do widely use the symmetry for atomic orbitals, point group symmetry, and advanced technique such as Racah algebra and its modifications for point group symmetry [23]. From the other hand the cluster model is an actual proving-ground for various calculation technique from simple quantum chemical MO-LCAO (molecular orbital-linear-combination-of-atomic-orbitals) method to a more elaborate LDA + MLFT (MLFT, multiplet ligand-field theory) [24] approach. The LDA + MLFT technique implies a sort of generalization of conventional ligand-field model with the DFT-based calculations. Haverkort *et al.* [24] start by performing a DFT calculation for the proper, infinite crystal using a modern DFT code which employs an accurate density functional and basis set [e.g., linear augmented plane waves (LAPWs)]. From the (self-consistent) DFT crystal potential they then calculate a set of Wannier functions suitable as the single-particle basis for the cluster calculation. The authors compared the theory with experimental spectra (XAS, nonresonant IXS, photoemission spectroscopy) for different 3d oxides and found overall satisfactory agreement, indicating that their ligand-field parameters are correct to better than 10%. However, the authors have been forced to treat on-site correlation parameter U_{dd} and orbitally averaged (spherical) Δ_{pd} parameter as adjustable ones. Despite the involvement of powerful calculation techniques the numerical results of the LDA + MLFT approach seem to be more like semiquantitative ones. Nevertheless, any comprehensive physically valid description of the electron and optical spectra for strongly correlated systems, as we suggest, should combine simple physically clear cluster ligand-field analysis with a numerical calculation technique such as LDA+MLFT [24], and a regular appeal to experimental data.

It is now believed that the most intensive low-energy electron-hole excitations in insulating 3d oxides correspond to the charge transfer (CT) transitions while different phonon-assisted crystal field transitions are generally much weaker. Namely the CT transitions are considered as a likely source of the optical and magneto-optical response of the 3d metal-based oxide compounds in a wide spectral range of 1-10 eV, in particular, of the fundamen-

tal absorption edge. The low-energy dipole-forbidden $d-d$ orbital excitations, or crystal field transitions, are characterized by the oscillator strengths which are smaller by a factor $10^2 - 10^3$ than those for the dipole-allowed $p-d$ CT transitions and usually correspond to contributions to the dielectric function ϵ'' of the order of 0.001-0.01.

Despite CT transitions are well established concept in the solid state physics, their theoretical treatment remains rather naive and did hardly progress during last decades. Usually it is based on the *one-electron* approach with some $2p-3d$ or, at best, $2p \rightarrow 3d t_{2g}$, $2p \rightarrow 3d e_g$ CT transitions in 3d oxides. In terms of the Hubbard model, this is a CT transition from the nonbonding oxygen band to the upper Hubbard band. But such a simplified approach to CT states and transitions in many cases appears to be absolutely insufficient and misleading even for qualitative explanation of the observed optical and magneto-optical properties. First, one should generalize the concept of CT transitions taking into account the conventional transition between the lower and upper Hubbard bands which corresponds to an inter-site $d-d$ CT transition, or intersite transition across the Mott gap.

Several important problems are hardly addressed in the current analysis of optical spectra, including the relative role of different initial and final orbital states and respective CT channels, strong intra-atomic correlations, effects of strong electron and lattice relaxation for CT states, the transition matrix elements, or transition probabilities, probable change in crystal fields and correlation parameters accompanying the charge transfer.

One of the central issues in the analysis of electron-hole excitations is whether low-lying states are comprised of free charge carriers or excitons. A conventional approach implies that if the Coulomb interaction is effectively screened and weak, then the electrons and holes are only weakly bound and move essentially independently as free charge-carriers. However, if the Coulomb interaction between electrons and holes is strong, excitons are believed to form, i.e. bound particle-hole pairs with strong correlation of their mutual motion.

Despite all the shortcomings the cluster models have proven themselves to be reliable working models for strongly correlated systems such as 3d compounds. These have a long and distinguished history of application in electron, optical and magneto-optical spectroscopy, magnetism, and magnetic resonance. The author with colleagues has successfully demonstrated great potential of the cluster model for description of the $p-d$ and $d-d$ charge transfer transitions and their contribution to optical and magneto-optical response in various 3d oxides such as ferrites [25–34], cuprates [35–39], manganites [34, 40, 41], and nickelates [42, 43].

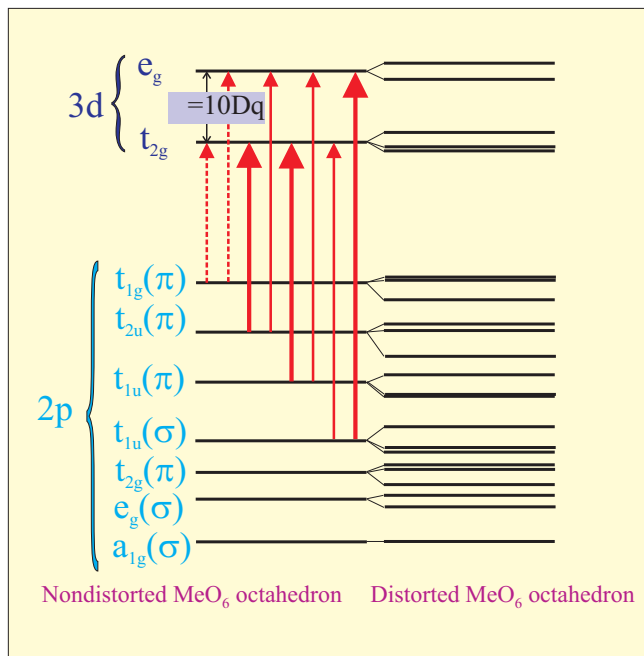


FIG. 1. The diagram of Me 3d-O 2p molecular orbitals for the MeO_6 octahedral center. The O 2p - Me 3d charge transfer transitions are shown by arrows: strong dipole-allowed $\sigma - \sigma$ and $\pi - \pi$ by thick solid arrows; weak dipole-allowed $\pi - \sigma$ and $\sigma - \pi$ by thin solid arrows; weak dipole-forbidden low-energy transitions by thin dashed arrows, respectively.

III. CLUSTER MODEL: THE CT CONFIGURATIONS AND CT TRANSITIONS IN FERRITES

A. Electronic structure of octahedral $[\text{FeO}_6]^{9-}$ clusters in ferrites

The slightly distorted octahedral $[\text{FeO}_6]^{9-}$ clusters are main optical and magneto-optical centers in weak ferromagnetic orthoferrites RFeO_3 , hematite $\alpha\text{-Fe}_2\text{O}_3$, borate FeBO_3 , cubic antiferromagnetic garnets like $\text{Ca}_3\text{Fe}_2\text{Ge}_3\text{O}_{12}$, and, together with tetrahedral $[\text{FeO}_4]^{5-}$ complexes in other ferrites as well.

Five Me 3d and eighteen oxygen O 2p atomic orbitals in octahedral MeO_6 complex with the point symmetry group O_h form both hybrid Me 3d-O 2p bonding and antibonding e_g and t_{2g} molecular orbitals, and purely oxygen nonbonding $a_{1g}(\sigma)$, $t_{1g}(\pi)$, $t_{1u}(\sigma)$, $t_{1u}(\pi)$, $t_{2u}(\pi)$ orbitals (see, e.g., Refs.[3, 23, 40]). Nonbonding $t_{1u}(\sigma)$ and $t_{1u}(\pi)$ orbitals with the same symmetry are hybridized due to the oxygen-oxygen O 2p π - O 2p π transfer. The relative energy position of different nonbonding oxygen orbitals is of primary importance for the spectroscopy of the oxygen-3d-metal charge transfer. This is firstly determined by the bare energy separation $\Delta\epsilon_{2p\pi\sigma} = \epsilon_{2p\pi} - \epsilon_{2p\sigma}$ between O 2p π and O 2p σ electrons.

Since the O 2p σ orbital points towards the two neighboring positive 3d ions, an electron in this orbital has its

energy lowered by the Madelung potential as compared with the O 2p π orbitals, which are oriented perpendicular to the respective 3d-O-3d axes. Thus, Coulomb arguments favor the positive sign of the $\pi - \sigma$ separation $\epsilon_{p\pi} - \epsilon_{p\sigma}$ which numerical value can be easily estimated in frames of the well-known point charge model, and appears to be of the order of 1.0 eV. In a first approximation, all the $\gamma(\pi)$ states $t_{1g}(\pi)$, $t_{1u}(\pi)$, $t_{2u}(\pi)$ have the same energy. However, the O 2p π -O 2p π transfer yields the energy correction to bare energies with the largest value and positive sign for the $t_{1g}(\pi)$ state. The energy of the $t_{1u}(\pi)$ state drops due to a hybridization with the cation 4p $t_{1u}(\pi)$ state. In other words, the $t_{1g}(\pi)$ state is believed to be the highest in energy non-bonding oxygen state. For illustration, in Figure 1 we show the energy spectrum of the 3d-2p manifold in the octahedral complexes MeO_6 with the relative energy position of the levels according to the quantum chemical calculations [44] for the $[\text{FeO}_6]^{9-}$ octahedral complex in a lattice environment typical for perovskites such as LaFeO_3 . It should be emphasized one more that the top of the oxygen electron band is composed of O 2p π nonbonding orbitals that predetermines the role of the oxygen states in many physical properties of 3d perovskites.

The *conventional* ground state electronic structure of octahedral Fe^{3+}O_6 clusters is associated with the configuration of the completely filled O 2p shells and half-filled Fe 3d shell. The typical high-spin ground state configuration and crystalline term for Fe^{3+} in the octahedral crystal field or for the octahedral $[\text{FeO}_6]^{9-}$ center is $t_{2g}^3e_g^2$ and ${}^6A_{1g}$, respectively.

The excited CT configuration $\underline{\gamma}_{2p}^1 3d^{n+1}$ arises from the spin-conserving transition of an electron from the predominantly anionic molecular orbitals γ_{2p} into an empty 3d type MO (t_{2g} or e_g). The transition between the ground and the excited configuration can be presented as the intra-center p-d CT transition $\gamma_{2p} \rightarrow 3d(t_{2g}, e_g)$.

The p-d CT configuration consists of two partly filled molecular-orbital subshells, localized predominantly on 3d cation and ligands, respectively. The excited cation configuration ($3d^6$) nominally corresponds to the Fe^{2+} ion. Strictly speaking, the many-electron p-d CT configuration should be written as $t_{2g}^{n_1}e_g^{n_2}\underline{\gamma}_{2p}$ with $n_1 + n_2 = 6$, or $((t_{2g}^{n_1}e_g^{n_2})^{2S'+1}\Gamma'_g; \underline{\gamma}_{2p})^{2S+1}\Gamma$ ($S = S' \pm \frac{1}{2}$, $\Gamma \in \Gamma'_g \times \gamma_{2p}$, ${}^{2S+1}\Gamma$ is a crystal term of the CT configuration), if we make use of the spin and orbital quasimomentum addition technique [23].

B. Intra-center electric-dipole p-d CT transitions

The conventional classification scheme of the intra-center electric-dipole p-d CT transitions in the octahedral $[\text{FeO}_6]^{9-}$ clusters first of all includes the electric-dipole allowed transitions from the odd-parity oxygen $\gamma_u = t_{1u}(\pi)$, $t_{2u}(\pi)$, $t_{1u}(\sigma)$ orbitals to the even-parity iron

$3dt_{2g}$ and $3de_g$ orbitals, respectively. These one-electron transitions generate the many-electron ones ${}^6A_{1g} \rightarrow {}^6T_{1u}$, which differ by the crystalline term of the respective $3d^6$ configuration:

$$(t_{2g}^3 {}^4A_{2g}; e_g^2) {}^6A_{1g} \rightarrow ((t_{2g}^4; e_g^2) {}^5T_{2g}; \underline{\gamma_u}) {}^6T_{1u}, \quad (1)$$

$$(t_{2g}^3 {}^4A_{2g}; e_g^2) {}^6A_{1g} \rightarrow ((t_{2g}^3; e_g^3) {}^5E_g; \underline{\gamma_u}) {}^6T_{1u}, \quad (2)$$

for $\gamma_u \rightarrow 3dt_{2g}$ and $\gamma_u \rightarrow 3de_g$ transitions, respectively. We see that in contrast to the manganese centers $\text{Mn}^{3+}\text{O}_6^{9-}$ [40] each one-electron $\gamma_u \rightarrow 3dt_{2g}$ transition generates one many-electron CT transition.

MeO_6 octahedral center can be written with the aid of Wigner-Eckart theorem [23] as follows (see Ref. [40] for details)

$$\langle \gamma_u \mu | \hat{d}_q | \gamma_g \mu' \rangle = (-1)^{j(\gamma_u) - \mu} \begin{pmatrix} \gamma_u & t_{1u} & \gamma_g \\ -\mu & q & \mu' \end{pmatrix}^* \langle \gamma_u || \hat{d} || \gamma_g \rangle, \quad (3)$$

where $\begin{pmatrix} \cdot & \cdot & \cdot \\ \cdot & \cdot & \cdot \\ \cdot & \cdot & \cdot \end{pmatrix}$ is the Wigner coefficient for the cubic point group O_h [23], $j(\Gamma)$ is the so-called quasimomentum number, $\langle \gamma_u || \hat{d} || \gamma_g \rangle$ is the one-electron dipole moment submatrix element. The 3d-2p hybrid structure of the even-parity molecular orbital $\gamma_g \mu = N_{\gamma_g} (3d\gamma_g \mu + \lambda_{\gamma_g} 2p\gamma_g \mu)$ and a more simple form of purely oxygen odd-parity molecular orbital $\gamma_u \mu \equiv 2p\gamma_u \mu$ both with a symmetry superposition of the ligand O 2p orbitals point to a complex form of the submatrix element in (3) to be a sum of *local* and *nonlocal* terms composed of the one-site and two-site (*d-p* and *p-p*) integrals, respectively. In the framework of a simple "local" approximation that implies the full neglect of all many-center integrals

$$\begin{aligned} \langle t_{2u}(\pi) || \hat{d} || e_g \rangle &= 0; \langle t_{2u}(\pi) || \hat{d} || t_{2g} \rangle = -i\sqrt{\frac{3}{2}}\lambda_\pi d; \\ \langle t_{1u}(\sigma) || \hat{d} || t_{2g} \rangle &= 0; \langle t_{1u}(\sigma) || \hat{d} || e_g \rangle = -\frac{2}{\sqrt{3}}\lambda_\sigma d; \\ \langle t_{1u}(\pi) || \hat{d} || e_g \rangle &= 0; \langle t_{1u}(\pi) || \hat{d} || t_{2g} \rangle = \sqrt{\frac{3}{2}}\lambda_\pi d. \end{aligned} \quad (4)$$

Here, $\lambda_\sigma \sim t_{pd\sigma}/\Delta_{pd}$, $\lambda_\pi \sim t_{pd\pi}/\Delta_{pd}$ are *effective* covalency parameters for e_g, t_{2g} electrons, respectively, $d = eR_0$ is an elementary dipole moment for the cation-anion bond length R_0 . We see, that the "local" approximation results in an additional selection rule: it forbids the $\sigma \rightarrow \pi$, and $\pi \rightarrow \sigma$ transitions, $t_{1u}(\sigma) \rightarrow t_{2g}$, and $t_{1,2u}(\pi) \rightarrow e_g$, respectively, though these are dipole-allowed. In other words, in frames of this approximation only σ -type ($t_{1u}(\sigma) \rightarrow e_g$) or π -type ($t_{1,2u}(\pi) \rightarrow t_{2g}$) CT transitions are allowed. Hereafter, we make use of the terminology of "strong" and "weak" transitions for the dipole-allowed CT transitions going on the $\sigma - \sigma$, $\pi - \pi$,

TABLE I. Parameters (energies, oscillator strength, line width) of the dipole allowed intra-center CT transitions in octahedral (${}^6A_{1g} \rightarrow {}^6T_{1u}$, No.= 1-6) and tetrahedral (${}^6A_{1g} \rightarrow {}^6T_2$, No.= 7-13) clusters in $\text{Y}_3\text{Fe}_5\text{O}_{12}$ [26, 31]. E_{comp} and E_{fit} are the computed and fitted CT transition energies, respectively.

No.	Transition	E_{comp} (eV)	E_{fit} (eV)	$f (\times 10^{-3})$	Γ (eV)
1	$t_{2u} \rightarrow t_{2g}$	3.1	2.8	4	0.2
2	$t_{1u}(\pi) \rightarrow t_{2g}$	3.9	3.6	30	0.3
3	$t_{2u} \rightarrow e_g$	4.4	4.3	60	0.3
4	$t_{1u}(\sigma) \rightarrow t_{2g}$	5.1	4.8	40	0.3
5	$t_{1u}(\pi) \rightarrow e_g$	5.3	5.2	200	0.3
6	$t_{1u}(\sigma) \rightarrow e_g$	6.4	6.1	200	0.3
7	$1t_1 \rightarrow 2e$	3.4	3.4	30	0.4
8	$6t_2 \rightarrow 2e$	4.3	4.6	20	0.3
9	$1t_1 \rightarrow 7t_2$	4.5	4.7	40	0.3
10	$5t_2 \rightarrow 2e$	5.0	4.9	30	0.3
11	$6t_2 \rightarrow 7t_2$	5.4	5.1	20	0.3
12	$1e \rightarrow 7t_2$	5.6	5.6	10	0.3
13	$5t_2 \rightarrow 7t_2$	6.0	6.0	20	0.3

and $\pi - \sigma$, $\sigma - \pi$ channels, respectively. It should be emphasized that the "local" approximation, if non-zero, is believed to provide a leading contribution to transition matrix elements with corrections being of the first order in the cation-anion overlap integral. Moreover, the nonlocal terms are neglected in standard Hubbard-like approaches. Given typical cation-anion separations $\mathbf{R}_{MeO} \approx 4$ a.u. we arrive at values less than 0.1 a.u. even for the largest two-site integral, however, their neglect should be made carefully. Exps.(3),(4) point to likely extremely large dipole matrix elements and oscillator strengths for strong *p-d* CT transitions, mounting to $d_{ij} \sim e\text{\AA}$ and $f \sim 0.1$, respectively.

Hence, starting with three nonbonding purely oxygen orbitals $t_{1u}(\pi), t_{1u}(\sigma), t_{2u}(\pi)$ as initial states for one-electron CT, we arrive at six many-electron dipole-allowed CT transitions ${}^6A_{1g} \rightarrow {}^6T_{1u}$. There are two transitions $t_{1u}(\pi), t_{2u}(\pi) \rightarrow t_{2g}$ ($\pi - \pi$ channel), two transitions $t_{1u}(\pi), t_{2u}(\pi) \rightarrow e_g$ ($\pi - \sigma$ channel), one transition $t_{1u}(\sigma) \rightarrow t_{2g}$ ($\sigma - \pi$ channel), and one transition $t_{1u}(\sigma) \rightarrow e_g$ ($\sigma - \sigma$ channel).

It should be noted that the dipole-forbidden $t_{1g}(\pi) \rightarrow t_{2g}$ transition seemingly determines the onset energy of all the p-d CT bands.

For our analysis to be more quantitative we make two rather obvious model approximations. First of all, we assume that as usually for cation-anion octahedra in 3d oxides [3, 44, 45] the non-bonding $t_{1g}(\pi)$ oxygen orbital has the highest energy and forms the first electron removal oxygen state. Furthermore, to be definite we assume that the energy spectrum of the non-bonding oxygen states for $[\text{Fe}^{3+}\text{O}_6]^{9-}$ centers coincides with that calculated in Ref. [44] for $[\text{Fe}^{3+}\text{O}_6]^{9-}$ in orthoferrite LaFeO_3 , in other

words, we have (in eV):

$$\Delta(t_{1g}(\pi) - t_{2u}(\pi)) \approx 0.8; \Delta(t_{1g}(\pi) - t_{1u}(\pi)) \approx 1.8;$$

$$\Delta(t_{1g}(\pi) - t_{1u}(\sigma)) \approx 3.0.$$

Secondly, we choose for the Racah parameters $B = 0.09$ eV and $C = 0.32$ eV, the numerical values typical for the Fe^{3+} ion [3].

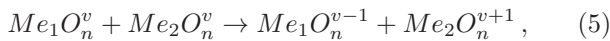
The energies of the intra-center CT transitions for octahedral FeO_6 and tetrahedral FeO_4 clusters in $\text{Y}_3\text{Fe}_5\text{O}_{12}$ were calculated using the spin-polarized X_α discrete variational (SP- X_α DV) method [26, 31]. These results are presented in Table I together with the results of fitting the experimental optical data [3, 46], taking into account only the contribution of the intra-center CT transitions with a Lorentzian line shape.

In addition to several dipole-allowed CT transitions, the CT band will also include various forbidden transitions. First of all, these are dipole-forbidden p-d transitions between states with the same parity of the $2pt_{1g}-3dt_{2g}$ type, as well as satellites of allowed transitions having the same electronic configuration, but different terms of the final states. For instance in the FeO_6 -octahedron, these are the ${}^6A_{1g} \rightarrow {}^6\Gamma_u$ transitions ($\Gamma = A_1, A_2, E, T_1$) forbidden by the quasimoment selection rule, and the ${}^6A_{1g} \rightarrow {}^4\Gamma_u$ spin forbidden transitions (if $\Gamma \neq T_{1u}$, then quasimoment forbidden, too). The forbiddenness of these transitions is lifted either by the electron-lattice interaction, low-symmetry crystal field, spin-orbital interaction, or the exchange interaction with neighbouring clusters. A detailed analysis of the energy spectrum of the CT band requires taking into account the d-d, p-d, and p-p correlation effects.

C. Inter-center $d-d$ CT transitions

Strictly speaking, reliable identification of the intra-center p-d CT transitions is possible only in highly dilute or impurity systems such as $\text{YAlO}_3:\text{Fe}$ or $\text{Ca}_3\text{Fe}_x\text{Ga}_{2-x}\text{Ge}_3\text{O}_{12}$, while in concentrated systems (YFeO_3 , $\text{Ca}_3\text{Fe}_2\text{Ge}_3\text{O}_{12}$, $\text{Y}_3\text{Fe}_5\text{O}_{12}$, ..) these transitions compete with inter-center d-d CT transitions [35–37, 39, 41, 42].

The inter-center $d-d$ CT transitions between two MeO_n clusters centered at neighboring sites 1 and 2 define inter-center $d-d$ CT excitons in 3d oxides [35–37, 39, 41, 42]. These excitons may be addressed as quanta of the disproportionation reaction



with the creation of electron MeO_n^{v-1} and hole MeO_n^{v+1} centers. Depending on the initial and final single particle states all the inter-center $d-d$ CT transitions may be classified to the $e_g - e_g$, $e_g - t_{2g}$, $t_{2g} - e_g$, and $t_{2g} - t_{2g}$ ones. For the 3d oxides with cations obeying the Hund rule

these can be divided to so-called high-spin (HS) transitions $S_1S_2S \rightarrow S_1 \pm \frac{1}{2}S_2 \mp \frac{1}{2}S$ and low-spin (LS) transitions $S_1S_2S \rightarrow S_1 - \frac{1}{2}S_2 - \frac{1}{2}S$, respectively.

An inter-center $d-d$ CT transition in iron oxides with Fe^{3+}O_6 octahedra



implies the creation of electron $[\text{FeO}_6]^{10-}$ and hole $[\text{FeO}_6]^{8-}$ centers with electron configurations formally related to Fe^{2+} and Fe^{4+} ions, respectively. The low-energy inter-center $d-d$ CT transitions from the initial $\text{Fe}^{3+}\text{O}_6(t_{2g}^3e_g^2) : {}^6A_{1g}$ states can be directly assigned to $e_g \rightarrow e_g$, $e_g \rightarrow t_{2g}$, $t_{2g} \rightarrow e_g$, and $t_{2g} \rightarrow t_{2g}$ channels with final configurations and terms

$$\begin{aligned} e_g \rightarrow e_g &: t_{2g}^3e_g^1; {}^5E_g - t_{2g}^3e_g^3; {}^5E_g, \\ e_g \rightarrow t_{2g} &: t_{2g}^3e_g^1; {}^5E_g - t_{2g}^4e_g^2; {}^5T_{2g}, \\ t_{2g} \rightarrow e_g &: t_{2g}^2e_g^2; {}^5T_{2g} - t_{2g}^3e_g^3; {}^5E_g, \\ t_{2g} \rightarrow t_{2g} &: t_{2g}^2e_g^2; {}^5T_{2g} - t_{2g}^4e_g^2; {}^5T_{2g}. \end{aligned} \quad (7)$$

In the framework of high-spin configurations the $e_g \rightarrow t_{2g}$ CT transition has the lowest energy $\Delta = \Delta_{e_g \rightarrow t_{2g}}$, while the $e_g \rightarrow e_g$, $t_{2g} \rightarrow t_{2g}$, and $t_{2g} \rightarrow e_g$ transitions have the energies $\Delta + 10Dq(3d^6)$, $\Delta + 10Dq(3d^4)$, and $\Delta + 10Dq(3d^6) + 10Dq(3d^4)$, respectively. The transfer energy in the Fe^{3+} -based ferrites for the $e_g \rightarrow t_{2g}$ CT transition

$$\Delta_{e_g t_{2g}}^{\text{Fe-Fe}} = A + 28B - 10Dq$$

can be compared with a similar quantity for the $e_g \rightarrow e_g$ CT transition in Mn^{3+} -based manganite LaMnO_3

$$\Delta_{e_g e_g}^{\text{Mn-Mn}} = A - 8B + \Delta_{JT},$$

where Δ_{JT} is the Jahn-Teller splitting of the e_g levels in manganite. Given $B \approx 0.1$ eV, $Dq \approx 0.1$ eV, $\Delta_{JT} \approx 0.7$ eV, $\Delta_{e_g e_g}^{\text{Fe-Fe}} \approx 2.0$ eV (see, e.g., Ref. [48]) we get $A \approx 2.0$ eV, $\Delta_{e_g t_{2g}}^{\text{Fe-Fe}} \approx 4.0$ eV. In other words, the onset of the $d-d$ CT transitions in Fe^{3+} -based ferrites is strongly (~ 2 eV) blue-shifted as compared to the Mn^{3+} -based manganite LaMnO_3 .

Another important difference between ferrites and manganites lies in the opposite orbital character of initial and final states for the $d-d$ CT transitions. Indeed, the low-energy $d^4d^4 \rightarrow d^3d^5$ CT transition in manganites implies an orbitally degenerate Jahn-Teller initial state ${}^5E_g {}^5E_g$ [49] and an orbitally nondegenerate final state ${}^4A_{2g} {}^6A_{1g}$ while the low-energy $d^5d^5 \rightarrow d^4d^6$ CT transitions in ferrites imply an orbitally nondegenerate initial state ${}^6A_{1g} {}^6A_{1g}$ and an orbitally degenerate Jahn-Teller final states such as ${}^5E_g {}^5E_g$ for $e_g \rightarrow e_g$ or ${}^5E_g {}^5T_{2g}$ for $e_g \rightarrow t_{2g}$ CT transitions. An unconventional final state with an orbital degeneracy on both sites, or Jahn-Teller excited states may be responsible for the complex multiplet lineshape of the inter-center $d-d$ CT band in ferrites.

D. Interplay of the CT transitions in ferrites

The most complete and detailed analysis of the optical spectra for a wide range of ferrites has been carried out in relatively recent papers [33, 34]. The authors analyze optical ellipsometry data in the spectral range of 0.6-5.8 eV for two groups of the iron oxides with more or less distorted FeO_6 octahedral and FeO_4 tetrahedral clusters. One of the two groups of materials includes orthoferrites RFeO_3 , bismuthate BiFeO_3 , $\text{Y}_{0.95}\text{Bi}_{0.05}\text{FeO}_3$, hematite $\alpha\text{-Fe}_2\text{O}_3$, $\text{Fe}_{2-x}\text{Ga}_x\text{O}_3$, and borate Fe_3BO_6 in which iron Fe^{3+} ions occupy only octahedral centro- or noncentrosymmetric positions and distortions range from 1 to 20 %. The second group includes lithium ferrite LiFe_5O_8 , barium hexaferrite $\text{BaFe}_{12}\text{O}_{19}$, iron garnets $\text{R}_3\text{Fe}_5\text{O}_{12}$, and calcium ferrite $\text{Ca}_2\text{Fe}_2\text{O}_5$ in which Fe^{3+} ions occupy both octahedral and tetrahedral positions with a rising tetra/ortho ratio. Experimental data were discussed within the cluster model which implies an interplay of intra- (p - d) and inter-center (d - d) CT transitions.

Some previously reported optical data on ferrites were in most cases obtained with the use of conventional reflection and absorption methods. The technique of optical ellipsometry provides significant advantages over conventional reflection and transmittance methods in that it is self-normalizing and does not require reference measurements. The optical complex dielectric function $\varepsilon = \varepsilon' - i\varepsilon''$ is obtained directly without a Kramers-Krönig transformation. The dielectric function ε was obtained in the range from 0.6 to 5.8 eV at room temperature. The comparative analysis of the spectral behavior of ε' and ε'' is believed to provide a more reliable assignment of spectral features. The spectra were analyzed using the set of the Lorentz functions

To begin our discussion of the CT transitions in ferrites we refer to the spectroscopic data for garnets $\text{Y}_3\text{Fe}_x\text{Ga}_{5-x}\text{O}_{12}$ ($x=5, 3.9, 0.29, 0.09$) [51]. They demonstrate that the optical response in the spectral range up to $30\,000\text{ cm}^{-1}$ ($\sim 3.7\text{ eV}$) is governed by the intra-center transitions for both octahedral and tetrahedral Fe^{3+} centers. It means that the onset energy for different d - d CT transitions in ferrites is expected to be $> 3.7\text{ eV}$ in agreement with our model estimates discussed in Sec.3.3.

To uncover the role played by the octahedral Fe^{3+} centers we turn to the optical response of the orthoferrites RFeO_3 .

These compounds contain the only type of centrosymmetric, slightly ($\sim 1\%$) distorted, FeO_6 octahedra. Despite the long story of optical and magneto-optical studies (see, e.g. Refs. [3, 52]) the microscopic origin of the main spectral features in orthoferrites remains questionable and the transition assignments made earlier in Ref. [3] need a comprehensive revisit. The $\varepsilon', \varepsilon''$ spectra of ErFeO_3 for three main polarizations shown in Fig. 2 are typical for orthoferrites RFeO_3 [3, 52, 53]. The low-energy intense band around 3 eV may be assigned to a strong dipole allowed intra-center $t_{2u}(\pi) \rightarrow t_{2g}$ CT transition as was proposed in Ref. [3]. This is a characteristic

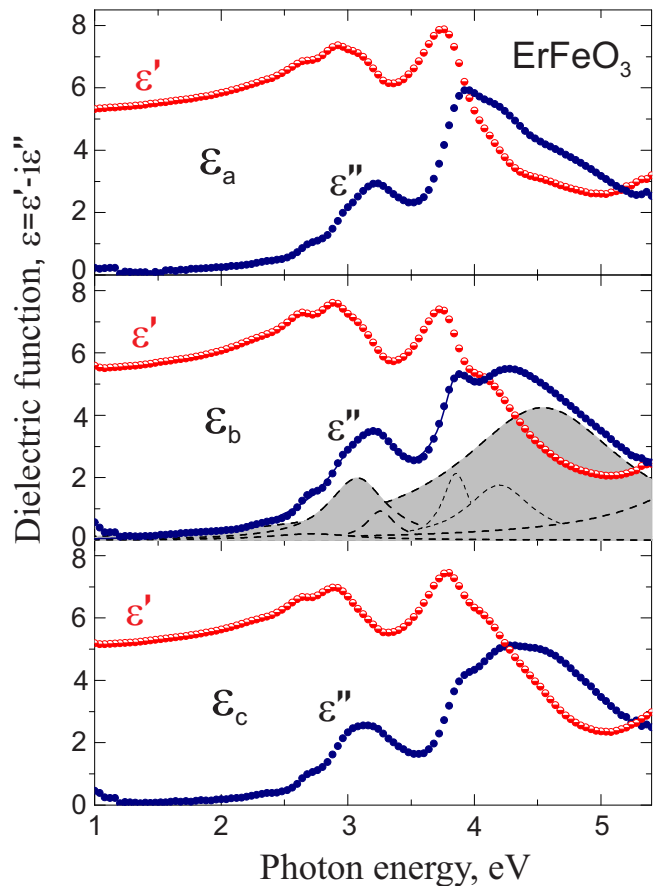


FIG. 2. (Color online) The dielectric function spectra in ErFeO_3 orthoferrite for three main polarizations. The Lorentzian fitting is marked by dotted curves and filling. Insets show indices of absorption and refraction.

feature of the octahedral Fe^{3+} centers in oxides. However, such an assignment also implies the existence of a weak band due to a low-energy dipole-forbidden intra-center $t_{1g}(\pi) \rightarrow t_{2g}$ CT transition, red-shifted by about 0.8 eV as expected from estimates [44]. Indeed, a band around 2.5 eV is found in the optical and magneto-optical spectra of different orthoferrites [3]. This band is clearly visible in hematite $\alpha\text{-Fe}_2\text{O}_3$ near 2.4 eV [33, 34] where the $t_{1g}(\pi) \rightarrow t_{2g}$ transition becomes allowed due to a breaking of the centro-symmetry for Fe^{3+} centers.

The nearest high-energy neighborhood of the 3 eV band is expected to be composed of $t_{1u}(\pi) \rightarrow t_{2g}$ CT transitions with a comparable intensity and estimated energy about 4 eV. All the dipole-allowed intra-center p - d CT transitions to the e_g state are blue-shifted by $10Dq(3d^5)$ as compared to their $\gamma \rightarrow t_{2g}$ counterparts with the onset energy of the order of 4 eV. Interestingly, for the dipole-allowed $\gamma_u \rightarrow t_{2g}$ transitions the maximum intensity is expected for the low-energy $t_{2u}(\pi) \rightarrow t_{2g}$ transition while for $\gamma_u \rightarrow e_g$ transitions the maximum intensity is expected for the high-energy ($\sim 6 - 7\text{ eV}$) $t_{1u}(\sigma) \rightarrow e_g$ transition. The analysis of the experimental spectra for orthoferrites demonstrates the failure of

the intra-center p - d CT transitions to explain the broad intensive band centered near 4.5 eV together with a narrow low-energy satellite peaked near 3.9 eV. Both features are typical for orthoferrites [3, 52] and may be assigned to a $e_g \rightarrow t_{2g}$ low-energy inter-center CT transition ${}^6A_{1g}{}^6A_{1g} \rightarrow {}^3E_g{}^5T_{2g}$ to an unconventional final state with an orbital degeneracy on both sites. These Jahn-Teller excited states are responsible for the complex lineshape of the $e_g \rightarrow t_{2g}$ CT band which is composed of a narrow exciton-like feature and a broad intense band separated by ~ 0.5 eV, which is believed to be a measure of the Jahn-Teller splitting in the excited state. Thus we see that all the spectral features observed in the optical spectra of orthoferrites for energies below 5 eV can be directly assigned to the low-energy intra-center p - d and inter-center d - d CT transitions.

It is worth noting that the dielectric function in orthoferrites is nearly isotropic due to very weak ($\sim 1\%$) rhombic distortions of FeO_6 octahedra and nearly equivalent different Fe-O-Fe bonds. Nevertheless a fine structure of the main CT bands is clearly revealed in magneto-optical spectra of orthoferrites, which was earlier assigned to the dipole-forbidden d - d crystal field transitions [3, 52]. In our opinion, their relation to the low-symmetry distortions in the p - d CT band seems to be more reasonable.

The effect of a strong change in bulk crystalline symmetry and local trigonal noncentrosymmetric distortions of FeO_6 octahedra is well illustrated by the optical response of hematite α - Fe_2O_3 [33, 34]. First of all there is a noticeable rise of intensity and a splitting for dipole-forbidden $t_{1g}(\pi) \rightarrow t_{2g}$ transition at 2.4 eV, which is clearly visible in the spectra of the gallium-substituted sample. Second, one should note a clear splitting on the order of 0.3-0.4 eV of the 3 eV band due to a sizeable trigonal distortion of the FeO_6 octahedra. In both cases the

band splitting effect reflects the singlet-doublet splitting of the initial orbital triplets, $t_{1g}(\pi)$ and $t_{2u}(\pi)$, respectively, due to the low-symmetry trigonal crystal field. Interestingly, the integral intensity of the $t_{2u}(\pi) \rightarrow t_{2g}$ band at 3 eV is visibly enhanced in hematite as compared to similar bands in orthoferrites that may result from the more covalent Fe-O bonding in hematite.

IV. EFFECTIVE HAMILTONIAN FOR FE-CLUSTERS IN FERRITES

As the principal interactions determining the CT transitions contribution to the optics and magneto-optics of ferrites, we note the symmetry crystal field ($LSCF$), Zeeman interaction V_Z , spin-orbit interaction V_{SO} , exchange interaction V_{ex} , and the exchange-relativistic interactions V_{so}^{ex} . The CT configurations have two unfilled shells – the $3d^6$ ($t_{2g}^4 e_g^2$ or $t_{2g}^3 e_g^3$) - shell and γ_{2p} - shell ($\tilde{\gamma}_{2p}^1$ -hole), which distinguishes them considerably from the ground state configuration having only one unfilled shell $3d^5$ ($t_{2g}^3 e_g^2$) and leads to the specificity of the manifestation of various interactions, especially anisotropic ones. Below, we consider the aforementioned interactions in the cluster approach.

A. Low-symmetry crystal field

Using the the cubic group irreducible tensor operator technique, in particular, the Wigner-Eckart theorem [23] we can write the matrix of the effective Hamiltonian of the low-symmetry crystal field, \hat{H}_{LSCF} , in general as follows

$$\langle \kappa S M_s \Gamma M | \hat{H}_{LSCF} | \kappa' S' M'_s \Gamma' M' \rangle = \sum_{\gamma\nu} \sum_{\Gamma'} B_{\nu}^{\gamma*} (\kappa \Gamma \kappa' \Gamma') (-1)^{\Gamma-M} \begin{pmatrix} \Gamma & \gamma & \Gamma' \\ -M & \nu & M' \end{pmatrix} \delta_{SS'} \delta_{M_s M'_s}, \quad (8)$$

where $\gamma = E, T_2$, $\langle :::: \rangle$ is the 3Γ symbol [23], κ, κ' are certain CT configurations, $B_{\nu}^{\gamma}(\Gamma\Gamma')$ are crystal field parameters.

For a certain T_1 (T_2) term the \hat{H}_{LSCF} can be written as an effective operator

$$V_{LSCF} = \sum_{ij} B_{ij}^{CF} \left[\widetilde{L_i L_j} - \frac{1}{3} L(L+1) \delta_{ij} \right]. \quad (9)$$

Here, B_{ij}^{CF} is the symmetric traceless matrix of the $LSCF$ parameters; $\widetilde{L_i L_j} = (L_i L_j + L_j L_i)/2$, \mathbf{L} is the effective orbital moment of the T_1 -, T_2 - term ($L = 1$). However, in general, the $LSCF$ can lead to the mixing of different cubic terms ${}^{2S+1}\Gamma$, ${}^{2S+1}\Gamma'$ ($E, T_2 \in \Gamma \times \Gamma'$) of identical or different CT configurations with

the same spin multiplicity. All these effects may be of importance, since H_{LSCF} reaches the magnitude up to ~ 0.1 eV under the low-symmetry distortions of the $[\text{FeO}_6]^{9-}$ complex of order 10^{-2} .

B. Conventional spin-orbital interaction

The conventional "intra-center" spin-orbital interaction $V_{SO} = \sum_i a(r_i) \mathbf{l}_i \cdot \mathbf{s}_i$ for a certain T_1 (T_2) term can be written as follows

$$V_{so} = \lambda \mathbf{L} \cdot \mathbf{S}, \quad (10)$$

where λ is the effective spin-orbit coupling constant, tabulated for the CT states of the $[\text{FeO}_6]^{9-}$, $[\text{FeO}_4]^{5-}$

clusters in Refs.[26, 31]. The contributions to λ are due both to the ligand (oxygen) 2p-subsystem and the iron subsystem, the latter contribution being dominant. V_{SO} leads to the terms splitting and mixing, the latter being especially significant in case of identical configurations or those differing from each other in the state of the 3d-shell, only. However, in general, the V_{SO} can lead to the mixing of different cubic terms ${}^{2S+1}\Gamma, {}^{2S'+1}\Gamma'$ ($|S-S'| \leq 1 \leq S+S'; T_1 \in \Gamma \times \Gamma'$).

C. Zeeman interaction

The Zeeman interaction $V_Z = \sum_i \mu_B (\mathbf{l}_i + 2\mathbf{s}_i) \cdot \mathbf{H}$ can be written for a certain $T_1 (T_2)$ term as an effective operator

$$V_Z = \mu_B (g_L \mathbf{L} + g_S \mathbf{S}) \cdot \mathbf{H}, \quad (11)$$

where g_S and g_L are respectively the spin g -factor ($g_S \approx 2$) and the effective orbital g -factor whose values are listed in Refs.[26, 31]. Note, that g_L can disagree with the classical orbital value $g_L = 1$ not only in magnitude, but even in sign. In particular, the CT state of the $t_{2u}^5 (t_{2g}^4 e_g^2 {}^5T_2)$ configuration dominating the magneto-optics of ferrites at the long wavelength tail, has the value $g_L = -\frac{3}{4}$. It is worth noting that at variance with the spin-orbital coupling the contributions to g_L due to the oxygen $\tilde{\gamma}_{2p}$ -hole and the 3d-electrons have comparable values.

D. Exchange interaction

The Heisenberg exchange interaction of the $[\text{FeO}_6]^{9-}$ m -cluster in the CT state with the neighbouring n -cluster in the ground ${}^6A_{1g}$ state can be written in a simplified form as follows

$$V_{ex} = -2 \sum_{m>n} J_{mn} (\mathbf{S}_m \cdot \mathbf{S}_n), \quad (12)$$

where J_{mn} is the exchange integral, although in general it should be replaced by the orbital operator, e.g. for a

certain ${}^6T_{1u}$ term for the m -cluster

$$\hat{J}_{mn} = J_{mn}^0 + \sum_{i=\alpha\beta} J_{mn}^{\alpha\beta} (\hat{L}_\alpha \hat{L}_\beta - \frac{2}{3} \delta_{\alpha\beta}). \quad (13)$$

In general, the cluster spin momentum operators in (12) should be replaced by the first rank spin operators, which can change the spin multiplicity. The V_{ex} gives rise to the orbital and spin splitting and mixing of the CT configuration terms. The exchange parameters in V_{ex} are determined not only by the ordinary cation-anion-cation superexchange $F e^{3+} - O^{2-} - F e^{3+}$, but also by the considerably stronger direct cation-anion $F e^{3+} - O^{2-}$ exchange reaching the magnitude on the order $\sim 0.1 eV$. Strictly speaking, at variance with the antiferromagnetic exchange interaction between the ground states the exchange in the CT state can lead to both antiferro- and ferromagnetic spin coupling. Interestingly, the matrix of the orbital operator \hat{J}_{mn} in (13) has a structure similar to V_{LSCF} (8) with the main orbitally isotropic $\gamma = A_{1g}$ term included. In other words, nontrivial orbital part of \hat{V}_{ex} can be considered as a spin-dependent contribution to the low-symmetry crystal field.

It should be noted that, in addition to the spin-dependent part, the exchange interaction also contains a spin-independent contribution, which has a similar orbital structure.

E. Exchange-relativistic interactions

Combined effect of a conventional intra-center spin-orbital coupling and orbitally nondiagonal exchange coupling for an excited orbitally degenerated state of the Fe-cluster within the second-order perturbation theory can give rise to a novel type of exchange-relativistic interaction, modified spin-orbital coupling \hat{V}_{SO}^{ex} , which can be written as a sum of isotropic, anisotropic antisymmetric, and anisotropic symmetric intra-center and inter-center terms, respectively [25, 26, 31, 54]

$$\hat{V}_{SO}^{ex} = \sum_{m,n} \lambda_{mn}^{(0)} (\mathbf{L}_m \cdot \mathbf{S}_n) + \sum_{m,n} (\lambda_{mn} \cdot [\mathbf{L}_m \times \mathbf{S}_n]) + \sum_{m,n} (\mathbf{L}_m \overset{\leftrightarrow}{\lambda}_{mn} \mathbf{S}_n). \quad (14)$$

It is worth noting that λ_{mn} has the symmetry of the Dzyaloshinskii vector [55–58], while the last term has the symmetry of the two-ion quasidipole spin anisotropy. Generally speaking, all the three terms can be of a comparable magnitude.

The contribution to the intra-center ($m = n$) bilinear interaction is determined by the spin-independent purely

orbital exchange, while the inter-center ($m \neq n$) term, or "spin-other-orbit" coupling \hat{V}_{SoO} , is determined by the spin-dependent exchange interaction. However, the spin-dependent exchange leads to the occurrence of additional nonlinear spin-quadratic terms, the contribution of which can be taken into account by the formal replacement of the linear spin operator \mathbf{S}_n in (14) for the nonlinear op-

erator \mathbf{S}_{mn}

$$\hat{S}_q(mn) = \hat{S}_q(n) + \gamma \left[\hat{V}^2(S(m)) \times S^1(n) \right]_q^1 = \hat{S}_q(n) + \gamma \sum_{q_1, q_2} \begin{bmatrix} 2 & 1 & 1 \\ q_1 & q_2 & q \end{bmatrix} \hat{V}_{q_1}^2(S(m)) S_{q_2}(n), \quad (15)$$

where $[\cdot\cdot\cdot]$ is the Clebsch-Gordan coefficient [59], $V_q^2(S)$ is the rank 2 spin irreducible tensor operator. In partic-

ular,

$$\hat{V}_0^2(S) = 2 \left[\frac{(2S-2)!}{(2S+3)!} \right]^{1/2} (3\hat{S}_z^2 - S(S+1)). \quad (16)$$

The coefficient γ in (15) can be calculated for specific terms. The isotropic part of V_{SoO} can be presented, in the general case, as follows

$$V_{SoO}^{iso} = \sum_{mn} \lambda(mn) (\mathbf{L}(m) \cdot \mathbf{S}(n)) + \sum_{m \neq n} \lambda'(mn) (\mathbf{L}(m) \cdot \mathbf{S}(m)) (\mathbf{S}(m) \cdot \mathbf{S}(n)). \quad (17)$$

Similarly to the Dzyaloshinskii vector, to estimate the parameters of the spin-other-orbit coupling, we can use the simple relation [60]

$$\lambda(m) \approx \lambda(mn) \approx \frac{\lambda' J'}{\Delta E_{S\Gamma}}, \quad (18)$$

where λ' and J' are the spin-orbital constant for the T_1 -, T_2 -states and the nondiagonal exchange parameter, respectively, $\Delta E_{S\Gamma}$ is a certain excitation energy. Parameters like $\lambda(m)$, $\lambda(mn)$ can be considerably larger than typical values of the Dzyaloshinskii vector [56–58], due both to smaller values of $\Delta E_{S\Gamma}$ and to the direct 2p–3d-exchange which, as stated above, is stronger than the 3d–2p–3d superexchange determining $\mathbf{d}(mn)$. Effective orbital magnetic fields acting on the T_1 and T_2 orbital states, e.g., for Fe^{3+} ions in ferrites due to V_{SO}^{ex} can reach the magnitude larger than 10 T ($\lambda' \geq 10^2 \text{ cm}^{-1}$, $J' \geq 10^2 \text{ cm}^{-1}$, $\Delta E_{S\Gamma} \sim 10^4 \text{ cm}^{-1}$).

The approach presented here can be immediately extended to tetrahedral clusters $[\text{FeO}_4]^{5-}$.

V. ANISOTROPIC POLARIZABILITY OF THE OCTAHEDRAL $[\text{FeO}_6]^{9-}$ -CLUSTER

Almost all ferrites are low anisotropic optical media in a wide spectral range : $\Delta\epsilon/\epsilon_0 \leq 10^{-2}$, ϵ_0 and $\Delta\epsilon$ being respectively the isotropic and anisotropic parts of the permittivity tensor $\hat{\epsilon}$. The latter can be written as the sum of the symmetric and antisymmetric parts:

$$\Delta\epsilon = \Delta\epsilon_{ij}^s + \Delta\epsilon_{ij}^a, \quad (19)$$

characterizing the linear birefringence/dichroism and the circular birefringence/dichroism, respectively. The latter can be described by axial gyration vector \mathbf{g} [61] which is dual to $\Delta\epsilon_{ij}^a$:

$$g_i = \frac{1}{2} e_{ijk} \Delta\epsilon_{jk}^a, \quad (20)$$

where e_{ijk} is the Levi-Civita tensor.

Within a linear approximation the Fe-cluster contribution to anisotropic permittivity tensor can be expressed in terms of the cluster anisotropic polarizability tensor $\hat{\alpha}$: as follows

$$\Delta\hat{\epsilon} = 4\pi N L \hat{\alpha}, \quad (21)$$

where N is the number of clusters per unit volume; $L = \frac{n_0^2 + 2}{9}$ is the Lorentz-Lorenz factor. Hence, for the gyration vector we have

$$\mathbf{g} = 4\pi N L \boldsymbol{\alpha}, \quad (22)$$

$\boldsymbol{\alpha}$ being the "microgyration vector", related to the antisymmetric part of the cluster polarizability tensor by an expression analogous to (20).

A. Simple microscopic theory

The microscopic analysis of the optical anisotropy is usually being carried out on the basis of the Kramers-Heisenberg formula [62] for the electronic polarizability; in case of the microgyration vector it takes on following

form :

$$\boldsymbol{\alpha} = \frac{1}{\hbar} \sum_{ij} \rho_i [\mathbf{d}_{ij} \times \mathbf{d}_{ji}] \cdot F_1(\omega, \omega_{ij}). \quad (23)$$

For the symmetric part of $\hat{\alpha}$, the Kramers-Heisenberg formula reduces to

$$\alpha_{kl}^{sym} = \frac{1}{\hbar} \sum_{ij} \rho_i \langle i|d_k|j\rangle \langle j|d_l|i\rangle \cdot F_2(\omega, \omega_{ij}). \quad (24)$$

In these formulae, \mathbf{d}_{ij} is the matrix element of the electric dipole moment \mathbf{d} ($d_{k,l}$ being its Cartesian projections) between the initial state $|i\rangle$ and the final state $|j\rangle$ for the CT transition; ρ_i is the statistical weight of the $|i\rangle$ state. F_k ($k=1,2$) is the Lorentz dispersion factor

$$F_k(\omega, \omega_{ij}) = \frac{(\omega + i\Gamma_{ij})[1 - (-1)^k] + \omega_{ij}[1 + (-1)^k]}{(\omega + i\Gamma_{ij})^2 - \omega_{ij}^2}. \quad (25)$$

Here, ω_{ij} denotes the CT transition frequency, Γ_{ij} is the line width.

Instead of the Cartesian tensor, one can introduce the

irreducible polarizability tensor [26, 31] :

$$\alpha_q^k = \frac{1}{\hbar} \sum_{ij} \sum_{q_1 q_2} \rho_i \begin{bmatrix} 1 & 1 & k \\ q_1 & q_2 & q \end{bmatrix} \langle i|d_{q_1}|j\rangle \langle j|d_{q_2}|i\rangle \cdot F_k(\omega, \omega_{ij}), \quad (26)$$

where $[\dots]$ is the Clebsch-Gordan coefficient [59], d_q is the irreducible tensor component of the dipole moment \mathbf{d} ($d_{\pm 1} = \mp \frac{1}{\sqrt{2}}(d_x \pm id_y)$, $d_0 = d_z$).

An important advantage of the irreducible tensor form is the natural separation of isotropic and anisotropic contributions: α_0^0 describes the isotropic refraction/absorption; α_q^1 and α_q^2 describe the circular and linear birefringence/dichroism, respectively.

For octahedral $[\text{FeO}_6]^{9-}$ (tetrahedral $[\text{FeO}_4]^{5-}$) clusters with an orbitally nondegenerate ground state ${}^6A_{1g}$ in ferrites, the contribution of the CT transitions ${}^6A_{1g} \rightarrow {}^6T_{1u}$ (${}^6A_{1g} \rightarrow {}^6T_2$) to the anisotropic polarizability will be associated only with certain "perturbations" in excited ${}^6T_{1u}$ - (6T_2 -) CT states.

In the linear approximation, we single out two main contributions $\alpha_q^k(\textit{split})$ and $\alpha_q^k(\textit{mix})$, associated with the orbital splitting of excited 6T -states and mixing/interaction of different 6T -states, respectively, under the action of various perturbations, V_{LSCF} , V_Z , V_{SO} , V_{SO}^{ex} [26, 31].

$$\alpha_q^k(\textit{split}) = \frac{1}{\hbar^2} \sum_{i={}^6A_{1g}} \sum_{j={}^6T_{1u}} \sum_{\mu\mu'} \sum_{q_1 q_2} \rho_i \begin{bmatrix} 1 & 1 & k \\ q_1 & q_2 & q \end{bmatrix} \times \langle i|d_{q_1}|j\mu\rangle \langle j\mu|\hat{V}|j\mu'\rangle \langle j\mu'|d_{q_2}|i\rangle \cdot \frac{\partial F_k(\omega, \omega_{ij}^0)}{\partial \omega_{ij}^{(0)}} \quad (27)$$

$$\alpha_q^k(\textit{mix}) = \frac{1}{\hbar} \sum_{i={}^6A_{1g}} \sum_{\substack{(j,j'={}^6T_{1u}) \\ E_j > E_{j'}}} \sum_{q_1 q_2} \rho_i \begin{bmatrix} 1 & 1 & k \\ q_1 & q_2 & q \end{bmatrix} \times \langle i|d_{q_1}|j\rangle \cdot \frac{\langle j|V|j'\rangle}{E_j - E_{j'}} \cdot \langle j'|d_{q_2}|i\rangle \cdot F_k(\omega, \omega_{ij}) \quad (28)$$

A simple illustration of the nature of circular and linear birefringence due to a splitting mechanism is presented in Figure 3.

Note that in ferrites with an orbitally nondegenerate ground ${}^6A_{1g}$ state of Fe-clusters, both linear and circular birefringence will be associated with orbital splitting/mixing in excited states. Obviously, the Fe-cluster contribution to the linear birefringence/dichroism will be related with low-symmetry crystal field V_{LSCF} in excited ${}^6T_{1u}$ states, while the contribution to circular birefringence/dichroism will be determined by the orbital Zeeman interaction or complex spin-orbital interaction such as V_{SO} and V_{SO}^{ex} . Large exchange spin fields up to 10^3 T and large spin Zeeman splittings do not make a direct contribution to circular magnetooptics in ferrites.

Due to a competition of the splitting and mixing mechanisms the spectral dependence of the polarizability cannot be considered to be a sum of separate individual

${}^6A_{1g} \rightarrow {}^6T$ CT transitions.

B. Symmetry considerations

Accounting for local point symmetry, crystal and magnetic symmetry in many cases provides important qualitative and even quantitative information about various anisotropic effects, in particular, the role of certain microscopic mechanisms.

1. Linear birefringence in orthoferrites

Simple symmetry considerations within the framework of the so-called "deformation" model made it possible to explain the dependence of linear birefringence on the type of R-ion in orthoferrites RFeO_3 [63].

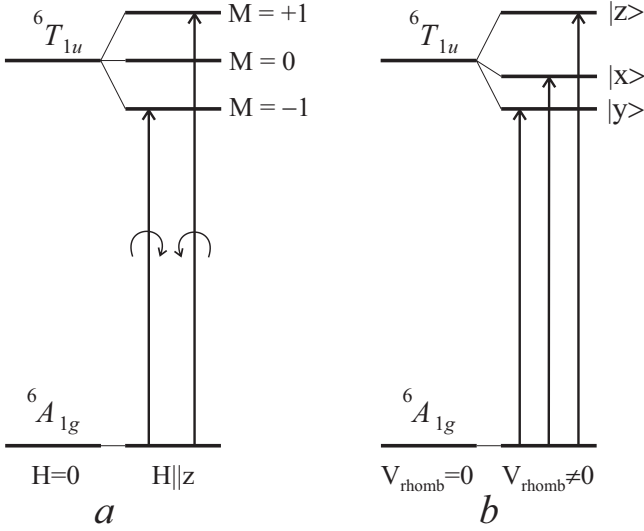


FIG. 3. An illustration of the nature of circular and linear birefringence due to a splitting mechanism: (a) schematic for the dipole allowed CT transitions ${}^6A_{1g} \rightarrow {}^6T_{1u}$ for the light with right and left circular polarization under external magnetic field and orbital *Zeeman* splitting; (b) schematic for the CT transitions ${}^6A_{1g} \rightarrow {}^6T_{1u}$ for the light with a linear polarization in a low-symmetry (rhombic) crystal field and *Stark* splitting for excited ${}^6T_{1u}$ state. Note that we are dealing with finite current (a) and currentless (b) states, respectively.

The real FeO_6 cluster in orthoferrites can be represented as a homogeneously deformed ideal octahedron. To find the degree of distortion, we introduce a symmetric strain tensor ε_{ij} according to the standard rules. In the local system of cubic axes of the octahedron

$$\varepsilon_{ij} = \frac{1}{4l^2} \sum_{n=1}^6 (R_i(n)u_j(n) + R_j(n)u_i(n)), \quad (29)$$

where $\mathbf{R}(n)$ is the radius-vector of the Fe-O_n bond, $\mathbf{u}(n)$ is the O_n -ligand displacement vector, or

$$\hat{\varepsilon} = \begin{pmatrix} 1 - \frac{l_1}{l} & \frac{1}{2}(\frac{\pi}{2} - \theta_{12}) & \frac{1}{2}(\frac{\pi}{2} - \theta_{13}) \\ \frac{1}{2}(\frac{\pi}{2} - \theta_{21}) & 1 - \frac{l_2}{l} & \frac{1}{2}(\frac{\pi}{2} - \theta_{23}) \\ \frac{1}{2}(\frac{\pi}{2} - \theta_{31}) & \frac{1}{2}(\frac{\pi}{2} - \theta_{32}) & 1 - \frac{l_3}{l} \end{pmatrix}, \quad (30)$$

where l is the Fe-O separation in an ideal octahedron, l_i are the Fe- O_i interatomic distances $\frac{1}{3}(l_1 + l_2 + l_3) = l$, and θ_{ij} are the bond angles $\text{O}_i\text{-Fe-O}_j$ in a real complex. Local x, y, z axes in octahedron are defined as follows: the z -axis is directed along the Fe-O_I , the x -axis is along Fe-O_{II} with the shortest Fe-O bond length. In general, the deformations of octahedra in orthoferrites are small and do not exceed 0.02.

Diagonal components of the traceless strain tensor (30) (tensile/compressive deformations) can be termed as E -type deformations since ε_{zz} and $\frac{1}{\sqrt{3}}(\varepsilon_{xx} - \varepsilon_{yy})$ transform according to the irreducible representation (irrep) E of the cubic group O_h , while off-diagonal components

(shear deformations) can be termed as T_2 -type deformations since ε_{yz} , ε_{xz} , and ε_{xy} transform according to the irrep T_2 of the cubic group O_h .

In the linear approximation, the symmetric anisotropic polarizability of the octahedron FeO_6 can be related to its deformation by the following relation

$$\alpha_{ij} = \begin{cases} p_E \varepsilon_{ij}, & i = j \\ p_{T_2} \varepsilon_{ij}, & i \neq j, \end{cases} \quad (31)$$

where ε_{ij} is the FeO_6 -octahedron deformation tensor ($\text{Tr} \hat{\varepsilon} = 0$); p_{E, T_2} are the photoelastic constants, relating the polarizability to E, T_2 -deformations, respectively. The relation (31) is valid in the local coordinate system of the FeO_6 -octahedron. In the abc -axes system, it can be rewritten as

$$\alpha_{ij} = p_E \varepsilon_{ij}^E + p_{T_2} \varepsilon_{ij}^{T_2}, \quad (32)$$

where ε_{ij}^E and $\varepsilon_{ij}^{T_2}$ are the components of the tensor of the E - and T_2 -deformations of the octahedron in the abc -system, respectively.

Proceeding to the permittivity tensor $\hat{\varepsilon}$ and summing over all Fe-ions sites, we arrive at nonzero diagonal components of $\hat{\varepsilon}$:

$$\varepsilon_{ii} = P_E \varepsilon_{ii}^E + P_{T_2} \varepsilon_{ii}^{T_2}, \quad (33)$$

where $P_{E, T_2} = 4\pi N \left(\frac{n_0^2 + 2}{3} \right)^2 p_{E, T_2}$; N is the number of Fe^{3+} ions per 1 cm^3 . Components of $\hat{\varepsilon}^E$, $\hat{\varepsilon}^{T_2}$ tensors serve as the *structure factors* and may be calculated taking into account the known components of the tensor of FeO_6 octahedron local deformations and the Eulerian angles relating the local axes to the abc ones.

Thus, we have a two-parameter formula (33) for the birefringence of orthoferrites as a function of rhombic distortions of their crystal structure. The photoelastic constants P_E, P_{T_2} can be found from the comparison of experimental data [64, 65] with the theoretical structure dependence of the ab -plane birefringence:

$$\Delta n_{ab} = n_a - n_b = \frac{1}{2n_0} [P_E(\varepsilon_{xx}^E - \varepsilon_{yy}^E) + P_{T_2}(\varepsilon_{xx}^{T_2} - \varepsilon_{yy}^{T_2})] \quad (34)$$

treated as a dependence on the type of the orthoferrite. The Figure 4 shows both experimental and calculated Δn_{ab} given $P_E = 6.2 n_0$, $P_{T_2} = 4.0 n_0$ (values obtained from the least-squares fitting). A very nice agreement of the two-parameter formula (34) with experiment testifies to the validity of the deformation model of the birefringence.

Using the found parameter P_{E, T_2} values, we are able to describe all the peculiarities of the orthoferrite birefringence. In particular, Figure 4 shows the theoretical predictions for the orientation angles $\pm\theta$ of optical axes, measured from the c -axis for the ac - and bc -planes and from the a -axis for the ab -plane, together with scarce experimental data on Eu, Tb, Dy, Y, Yb orthoferrites [65, 66]. Quite good agreement with the available

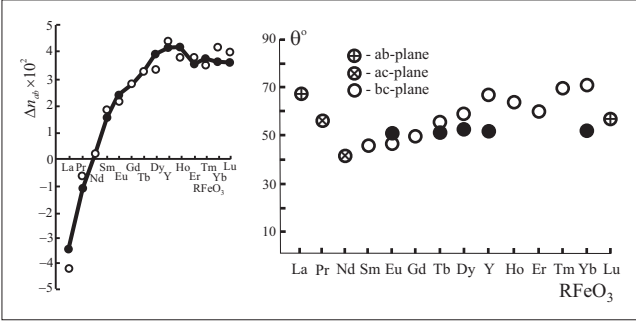


FIG. 4. Left panel: Linear birefringence Δn_{ab} for orthoferrites $RFeO_3$ in ab -plane, solid circles are predictions of the deformation model, hollow circles are experimental data ($\lambda = 0.633 \mu m$) [64]. Right panel: The orientation angles ($\pm\theta$) of optical axes in respective planes of orthoferrites predicted by the deformation model. The solid black circles are scarce experimental data for bc -plane ($\lambda = 0.68 \mu m$) [65, 66].

experimental data is another confirmation of the validity of the deformation model of birefringence of orthoferrites. In general, for all its simplicity, the deformation model reflects quite correctly the main peculiarities of the natural birefringence of orthoferrites.

2. Circular birefringence/dichroism in ferrites

The gyration vector and the magnetic moment (or the ferromagnetic vector \mathbf{m}) have the same transformation properties.

For *ferrimagnetic* iron garnets

$$\mathbf{g} = \hat{A}_a \mathbf{m}_a + \hat{A}_d \mathbf{m}_d + \hat{C} \mathbf{H}, \quad (35)$$

where \mathbf{m}_a and \mathbf{m}_d are magnetic moments, or ferromagnetic vectors, of octahedral and tetrahedral sublattices, respectively.

In weak ferromagnets like $RFeO_3$ and in a number of other magnetic compounds with non-equivalent magnetic sublattices, certain components of the ferromagnetic vector \mathbf{m} and the antiferromagnetic vector \mathbf{l} in a two-sublattice model transform identically, what enables one to write \mathbf{g} in the linear approximation through \mathbf{m} , \mathbf{l} , and the external magnetic field \mathbf{H} as

$$\mathbf{g} = \hat{A} \mathbf{m} + \hat{B} \mathbf{l} + \hat{C} \mathbf{H}, \quad (m^2 + l^2 = 1) \quad (36)$$

(the ferromagnetic (*FM*), antiferromagnetic (*AFM*), and field contributions, respectively)

The form of each of \hat{A} , \hat{B} , \hat{C} tensors is determined by the crystal symmetry. For example, in orthorhombic weak ferromagnetic orthoferrites $RFeO_3$

$$\hat{A} = \begin{pmatrix} a_{xx} & 0 & 0 \\ 0 & a_{yy} & 0 \\ 0 & 0 & a_{zz} \end{pmatrix}, \quad \hat{B} = \hat{B}^s + \hat{B}^a = \begin{pmatrix} 0 & 0 & b_{xz} \\ 0 & 0 & 0 \\ b_{zx} & 0 & 0 \end{pmatrix},$$

$$a_{xx} \neq a_{yy} \neq a_{zz}, \quad b_{zx} \neq b_{xz}.$$

In rhombohedral weak ferromagnets (α - Fe_2O_3 , $FeBO_3$, FeF_3 , etc.)

$$\hat{A} = \begin{pmatrix} a_{\perp} & 0 & 0 \\ 0 & a_{\perp} & 0 \\ 0 & 0 & a_{\parallel} \end{pmatrix}, \quad \hat{B} = \hat{B}^a = \begin{pmatrix} 0 & b_{xy} & 0 \\ b_{yx} & 0 & 0 \\ 0 & 0 & 0 \end{pmatrix},$$

i.e., $b_{yx} = -b_{xy}$, and the \hat{B} tensor, in contrast with orthoferrites, is antisymmetric. The symmetry properties of the \hat{A} and \hat{C} tensors are identical.

The special role of the antiferromagnetic contribution to the gyration vector for weak ferromagnets is due to the fact that for them, as a rule, $m \ll l$, for example, $m/l \approx 0.01$ in $YFeO_3$ and $m/l \approx 0.001$ in α - Fe_2O_3 , respectively [57, 58, 67]. However, the components of the gyration vector \mathbf{g} in α - Fe_2O_3 and $YFeO_3$ are comparable in magnitude with those for the yttrium iron garnet, $Y_3Fe_5O_{12}$ [3, 68] although the magnetization of the latter is approximately by two orders larger than in the hematite and by one order larger than in orthoferrites. It seems impossible to explain this phenomenon other than in terms of the *AFM* contribution. Hence, it appears that there must be microscopic mechanisms causing the antisymmetric relations of the gyration vector to spins :

$$\mathbf{g} = \sum_{mn} [\mathbf{B}(mn) \times \langle \mathbf{S}(n) \rangle], \quad (37)$$

where the vector $\mathbf{B}(mn)$ is determined by the antisymmetric part of \hat{B} .

VI. CHARGE TRANSFER TRANSITIONS AND MAGNETO-OPTICAL EFFECTS (MOE) IN FERRITES

A. Working microscopic models for circular MOE

The main contribution to the microgyration vector for $[FeO_6]^{9-}$ and $[FeO_4]^{5-}$ clusters and the circular MOE for ferrites is determined by the splitting and mixing mechanisms [26]. To the first order of the perturbation theory, only the interactions V_{SO} , V_Z , V_{SO}^{ex} play part, as these are odd in the orbital moment and enable the orbital splitting and mixing of excited CT states of the ${}^6T_{1u}$ type. Note that the spin part of V_Z just as the isotropic Heisenberg spin exchange of the $[FeO_6]^{9-}$ cluster with its magnetic surroundings, characterized by the spin exchange field H_{ex} , do not contribute in the linear approximation to the circular MOE. V_{SO} and the orbital part of V_Z yield the FM and field contributions to the gyration vector; their combined action for the "octahedral" CT transitions due to the splitting of the excited ${}^6T_{1u}$ states is given by

$$\mathbf{g}_a^{split} = 2 \sum_{j=6T_{1u}} \frac{\pi e^2 L N}{\hbar m_e \omega_{0j}} \left(\lambda^j \langle \mathbf{S} \rangle + \mu_B g_L^j \mathbf{H} \right) f_j \frac{\partial F_1(\omega, \omega_{0j})}{\partial \omega_{0j}}. \quad (38)$$

where $\langle \mathbf{S} \rangle$ is the thermodynamic spin average, f_j is the oscillator strength for ${}^6A_{1g} - {}^6T_{1u}$ CT transition, λ^j and g_L^j are effective spin-orbital constant and orbital g -factor for a certain ${}^6T_{1u}$ term (see tables 1 and 2 in Ref. [26]).

$$\mathbf{g}_a^{mix} = \sum_{\substack{(j,k=6T_{1u}) \\ (E_{0j} > E_{0k})}} \frac{4\pi e^2 LN}{m_e} \left(\lambda^{jk} \langle \mathbf{S} \rangle + \mu_B g_L^{jk} \mathbf{H} \right) \left(\frac{f_j f_k}{\omega_{0j} \omega_{0k}} \right)^{1/2} \langle {}^6A_{1g} \| d \| j \rangle \langle {}^6A_{1g} \| d \| k \rangle \frac{F_1(\omega, \omega_{0j}) - F_1(\omega, \omega_{0k})}{E_{0j} - E_{0k}} \quad (39)$$

where $\langle {}^6A_{1g} \| d \| j \rangle$ is the dipole moment submatrix element. The parameters of the type of effective orbital g -factors g_L^{jk} and spin-orbit coupling constants λ^{jk}

$$g_L^{jk} = \frac{\langle \kappa_j {}^6T_{1u} \| \sum_n \mathbf{l}_n \| \kappa_k {}^6T_{1u} \rangle}{\langle 1 \| \hat{l} \| 1 \rangle}; \quad g_L \equiv g_L^{jj} \equiv g_L^j \quad (40)$$

$$\lambda^{jk} = \frac{\langle \kappa_j {}^6T_{1u} \| \hat{Q}^{11} \| \kappa_k {}^6T_{1u} \rangle}{\langle 1 \| \hat{l} \| 1 \rangle \langle \frac{5}{2} \| \hat{s} \| \frac{5}{2} \rangle}; \quad \lambda \equiv \lambda^{jj} \equiv \lambda^j, \quad (41)$$

are determined by the submatrix elements of the sum $\sum_n \mathbf{l}_n$ of one-particle orbital moment operators acting on all atomic orbitals in the molecular orbitals, and by the submatrix element of the double irreducible spin-orbit tensor operator \hat{Q}^{11} [69]. Numerical values of g_L^{jk} and λ^{jk} for the CT states of the $[\text{FeO}_6]^{9-}$ and $[\text{FeO}_4]^{5-}$ clusters are given in Tables 1 and 2 [26]. In (40), (41), both the splitting ($j = k$) and mixing ($j \neq k$) are taken into account. κ_j is the set of intermediate quantum numbers, necessary for distinguishing different ${}^6T_{1u}$ terms. f_j is the oscillator strength of the ${}^6A_{1g} \rightarrow \kappa_j {}^6T_{1u}$ CT transition, E_{0j} is its energy.

Thus, V_{SO} and V_Z to the 1st order of the perturbation theory, give rise to *isotropic* \hat{A} , \hat{C} tensors (36). The frequency dependences of the real and imaginary parts of the splitting contribution to \mathbf{g} for a CT transition have respectively the "dissipative" and "dispersive" form.

The splitting contribution of the exchange-relativistic interaction V_{SO}^{ex} (14) for isolated ${}^6T_{1u}$ term to the gyration vector can be represented as follows [25, 26, 31, 54]:

$$\mathbf{g} = \frac{2\pi L e^2 f_{AT}}{m \hbar \omega_0} \left(\overset{\leftrightarrow}{\lambda} \langle \hat{\mathbf{S}} \rangle + \sum_n \overset{\leftrightarrow}{\lambda}_n \langle \hat{\mathbf{S}}_n \rangle \right) \frac{\partial F(\omega, \omega_0)}{\partial \omega_0}, \quad (42)$$

where first and second terms in brackets correspond to intra-center and inter-center, or spin-other-orbit exchange-relativistic contributions, respectively, $\overset{\leftrightarrow}{\lambda}$ and $\overset{\leftrightarrow}{\lambda}_n$ are the effective tensors of the respective interactions. In other words, these terms correspond to contributions with $m = n$ and $m \neq n$ in V_{SO}^{ex} (14). The summation over n in (42) extends to the nearest neighbors of the considered center, f_{AT} is the oscillator strength of the ${}^6A_{1g} - {}^6T_{1u}$ transition. In general, in accordance

The contribution of the mixing mechanism, that is of the interaction of different ${}^6T_{1u}$ CT terms of the octahedral $[\text{FeO}_6]^{9-}$ (6T_2 CT terms of the tetrahedral $[\text{FeO}_4]^{5-}$) cluster can be written as follows [26])

with (14) the tensors $\overset{\leftrightarrow}{\lambda}$ and $\overset{\leftrightarrow}{\lambda}_n$ of the intra- and inter-center exchange-relativistic contributions in (42) contain isotropic, antisymmetric, and symmetric anisotropic components.

In addition to the "gyroelectric" contribution to the gyration vector that we have considered, we should note the existence of a small "gyromagnetic" contribution related with the magnetic susceptibility, which determines the frequency-independent contribution to the Faraday rotation [70]

$$\Delta \Theta_F = \frac{2\pi n_0}{c} \gamma m, \quad (43)$$

where γ is gyromagnetic ratio, m is magnetic moment. It is interesting that yttrium iron garnet in the wavelength range $\lambda > 5 \mu m$ is a gyromagnetic medium, since the gyromagnetic contribution to the Faraday rotation is predominant ($\Theta_F \approx 60 \text{ deg/cm}$ at $T=300 \text{ K}$), although in the wavelength range $\lambda < 4 \mu m$ it can be considered as an ordinary gyroelectric medium due to a sharp increase in the gyroelectric contribution in Θ_F [70].

B. Fe^{3+} diluted nonmagnetic compounds

The most suitable objects for the application and justification of the cluster theory for ferrites are the Fe^{3+} diluted nonmagnetic compounds such as YAlO_3 and $\text{Ca}_3\text{Ga}_2\text{Ge}_3\text{O}_{12}$ with the crystal structure close to orthoferrite YFeO_3 and iron garnet $\text{Ca}_3\text{Fe}_2\text{Ge}_3\text{O}_{12}$, respectively. In such dilute systems, band models are inapplicable for describing Fe 3d states, so that the cluster model has virtually no competitors in describing the optical and magneto-optical response of dilute systems in the O 2p-Fe 3d charge transfer range, especially since it becomes possible to restrict ourselves to taking into account only intra-center p-d transfer.

The Faraday effect was measured in single-crystalline samples of diluted garnet $\text{Ca}_3\text{Ga}_{2-x}\text{Fe}_x\text{Ge}_3\text{O}_{12}$ ($x=0.15$) [25], where the Fe^{3+} ions occupy only the octahedral positions, and the $[\text{FeO}_6]^{9-}$ octahedrons are assumed to be essentially noninteracting. Making use of the splitting (38) and mixing (39) contributions to the gyration vector with the data for effective orbital g -factors and spin-orbital parameters from Table 1 in

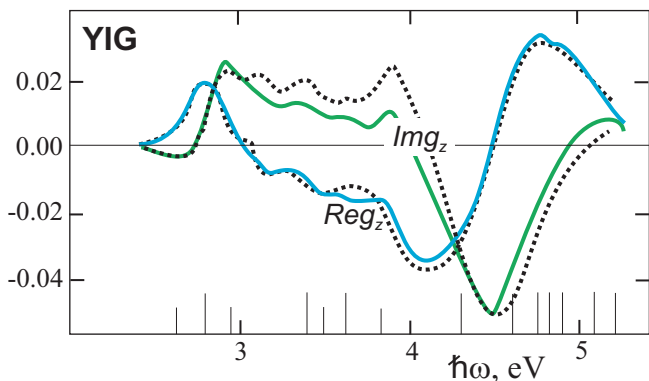


FIG. 5. Spectral dependence of the real and imaginary parts of the z -component of the gyration vector in YIG: experimental data are shown by dotted curves, model fitting is shown by solid curves.

Ref. [26] and assuming that energies of all "octahedral" CT transitions in this garnet are blue-shifted by 1.4 eV in comparison with corresponding energies in "orthoferrite" complexes (see Table I), the authors calculated both the ferromagnetic and field contributions to the Faraday rotation

$$\Theta_F = \frac{\omega}{2n_0 c} g = A_F m + C_F H, \quad (44)$$

over the entire CT band. As a result, good agreement was obtained with the experimental values of the ferromagnetic and field contributions to Θ_F , measured in the spectral range 1.4-3.1 eV (see Figure 2 in Ref. [25]).

Unfortunately, there are few examples in the literature of a systematic study of the concentration dependence of optical and magneto-optical effects in diluted systems.

C. The yttrium iron garnet

The absence of the magneto-optically active rare-earth sublattice in yttrium iron garnet $Y_3Fe_5O_{12}$ permits the evaluation of the "undistorted" iron sublattices contribution. In addition, experimental studies of YIG magneto-optics are abundant [3, 50, 51, 71]. The authors [26] have undertaken a theoretical model computation of the FM and field contributions (36) to the gyration vector of the YIG, taking into account the CT transitions both in octahedral $[FeO_6]^{9-}$ and tetrahedral $[FeO_4]^{5-}$ clusters.

Figure 5 shows the results of the theoretical simulation of the spectral dependence of the real and imaginary parts of the gyration vector z -component, $Re g_z$ and $Im g_z$, in YIG (solid lines), with dipole allowed and a number of dipole forbidden CT transitions (marked by long and short line segments at the bottom of the Figure 5, taken into account. The parameters of the main CT transitions used in the model simulation are presented in Table I. Besides a satisfactory agreement with the experimental data in a wide spectral range, 2.5 –

5.5 eV, the computed $Re g_z$ value on the long wavelength tail of the CT transitions band ($\lambda = 0.63 \mu m$) yields the Faraday rotation in YIG $\Theta_F = 860 \text{ deg/cm}$, practically coinciding with the experimental value 830 deg/cm [72, 73]. The computed values of the partial Faraday rotation contributions due to octahedral CT transitions (6500 deg/cm) and tetrahedral ones (-5640 deg/cm) satisfactorily agree with the experimental values 8670 and -7840 deg/cm , respectively [72, 73]. As expected for a longitudinal ferrimagnet, we see the effect of significant mutual compensation for the contributions of the octa- and tetra-sublattices.

Both in the octahedral CT transitions contribution to $Re g_z$, and in that of the tetrahedral transitions, the main role belongs to the mixing mechanism, in agreement with the predominance of paramagnetic-shaped lines in magneto-optical spectra of YIG noted in Ref. [74].

The authors [26] have also computed the field contribution (36) to the YIG gyration vector \mathbf{g} , with theoretical values of the orbital Landé factors g_L^{jk} (see Tables 1 and 2 in Ref. [26]), taking into account the main electric-dipole-allowed CT transitions, only. Rough as it is, the approximation of allowed CT transitions gives nevertheless the Θ_F/H values of $-10^\circ \cdot \text{cm}^{-1} \cdot T^{-1}$ ($\lambda = 0.7 \mu m$) and $-2.4^\circ \cdot \text{cm}^{-1} \cdot T^{-1}$ ($\lambda = 1.1 \mu m$) – near to corresponding experimental data ($-12.4^\circ \cdot \text{cm}^{-1} \cdot T^{-1}$ [75] and $-2.5^\circ \cdot \text{cm}^{-1} \cdot T^{-1}$ [76], respectively). The lack of experimental data precluded a comparison at shorter wavelengths.

The electronic structure, magnetic, optical and magneto-optical properties of yttrium iron garnet were investigated recently [8] by using "first principles" GGA+U calculations with Hubbard energy correction for the treatment of the strong electron correlation. The authors boldly make a too strong statement that "the calculated Kerr spectrum which included on-site Coulomb interaction of Fe 3d electrons described well the experimental results", which clearly does not follow from the data presented in Figure 6 from their article, especially since the calculated dielectric function shows a dramatic discrepancy with experiment.

D. Bi-substituted iron garnets

Although pure yttrium iron garnet has several advantages in terms of magneto-optical response, it has not been widely applied in integrated devices due to its limited Faraday rotation. However, decompensation of the contributions of the octa- and tetra-sublattices, in particular, due to the replacement of R-ions in $R_3Fe_5O_{12}$ garnets by Bi^{3+} or Pb^{3+} ions, makes it possible to increase the Faraday rotation of iron garnets by one or two orders of magnitude in the visible and near-infrared region (see, e.g., Ref. [46]).

Wittekoek et al. [46] proposed in a purely qualitative manner that the origin of the large Faraday rotation in Bi,Pb-substituted iron garnets is the hybridization of

Bi,Pb 6p orbitals, which possess anomalously large spin-orbit coupling ($\zeta_{6p} \approx 2$ eV), with the O 2p and Fe 3d orbitals. Later this idea was supported and developed within cluster molecular orbital theory [30, 32, 77]. The enhancement of spin-orbit coupling in Fe 3d orbitals was assumed to be much smaller than that in O 2p orbitals, because Fe sites are located more distant than O sites from Bi sites.

Taking account of the overlap of $2p(O^{2-})$ and $6p(Bi^{3+})$ electronic shells as well as the *virtual* transition of the oxygen $2p$ - electron to the bismuth empty $6p$ - shell, the wave function of the outer $2p$ - electrons of the neighboring oxygen ion acquires thereby an admixture of Bi 6p-states [30, 32]:

$$\varphi_{2p m} \longrightarrow \psi_{2p m} = \varphi_{2p m} - \sum_{m'} \langle 6p m' | 2p m \rangle^* \varphi_{6p m'} , \quad (45)$$

where $\varphi_{2p m}$ and $\varphi_{6p m}$ are atomic wave functions.

The Bi 6p-O 2p hybridization results in the modification of the spin-orbit interaction on the oxygen ion :

$$V_{SO} = V_{SO}(2p) + \Delta V_{SO}^{iso}(2p) + \Delta V_{SO}^{an}(2p) , \quad (46)$$

where $V_{SO}(2p) = \zeta_{2p} (\mathbf{l} \cdot \mathbf{s})$ is conventional spin-orbital interaction with $\zeta_{2p} \approx 0.02$ eV, $\Delta V_{SO}^{iso}(2p)$ and $\Delta V_{SO}^{an}(2p)$ are effective isotropic and anisotropic terms due to the Bi 6p-O 2p hybridization:

$$\Delta V_{SO}^{iso}(2p) = \Delta \zeta_{2p} (\mathbf{l} \cdot \mathbf{s}) , \quad (47)$$

where effective spin-orbital parameter is estimated in Ref. [32] to be $\Delta \zeta_{2p} \leq 0.1$ eV per one Bi^{3+} -ion, that is several times larger than conventional parameter ζ_{2p} :

$$\Delta V_{SO}^{an}(2p) = \lambda_{ij} \hat{l}_i \hat{s}_j , \quad (48)$$

where the effective spin-orbit interaction tensor λ_{ij} depends on the geometry of the Bi-O bond [30, 32]

$$\lambda_{ij} \propto \zeta_{6p} \left(R_i R_j - \frac{1}{3} \delta_{ij} \right) , \quad (49)$$

where \mathbf{R} is a unit vector along the Bi-O bond direction.

Thus, the effect of the bismuth ions on the circular MOE in iron garnets is essentially related to the oxygen O 2p-states in $[FeO_6]^{9-}$ and $[FeO_4]^{5-}$ clusters. The Bi^{3+} ions, leading to an increase in the effective spin-orbital coupling constant for oxygen ions, have a significant effect on the circular magneto-optics of iron garnets, through a change in the effective spin-orbital coupling parameters

$$\lambda = \lambda(3d) + \lambda(2p)$$

for the excited 6T -states with the p-d charge transfer.

The simple theory we are considering allows us to make a number of predictions. First, the effect of the Bi 6p-O 2p hybridization may be particularly significant for the CT transitions, whose final state spin-orbit coupling constant λ contains the ligand contribution $\lambda(2p)$

only, e.g., the transitions $t_{2u} - e_g$ and $t_{1u}(\pi) - e_g$ in the $[FeO_6]^{9-}$ clusters (predicted energies 4.4 and 5.3 eV, respectively). Since $\zeta_{2p} \ll \zeta_{3d} \approx 0.1$ eV the contribution of such transitions to the *FM* part of the gyration vector (36) in unsubstituted garnets is practically vanishing. The Bi substitution makes these transitions observable. On the contrary, the CT transitions whose final state V_{SO} constant λ includes only the 3d-contribution, e.g., transition $t_{1u}(\sigma) - e_g$ in the $[FeO_6]^{9-}$ clusters (predicted energy 6.4 eV) are not appreciably influenced by the Bi^{3+} -ions. Thus, the spectral dependence of the gyration vector in YIG and Bi-substituted compounds can differ greatly. Second, the Bi 6p-O 2p hybridization induces the anisotropy of the \hat{A} tensor in the FM contribution to the gyration vector (36), which differs for the octa- and tetra-positions of the Fe clusters. Third, in our model, bismuth ions do not directly affect the value of the field contribution $\hat{C} \mathbf{H}$ (36) to the gyration vector.

At variance with the cluster model, the "first-principles" band calculations indicate a slightly different, albeit contradictory, picture of Bi 6p-O 2p-Fe 3d hybridization. Thus, analyzing the electronic structure of $Bi_3Fe_5O_{12}$ (BIG) calculated by the fully relativistic first-principles method based on the full-potential linear-combination-of-atomic-orbitals (LCAO) approach within the local-spin-density-approximation (LSDA), Oikawa et al. [6] found that the enhancement of the spin-orbit coupling due to the hybridization of Bi 6p is considerably larger in the Fe 3d conduction bands than in the O 2p and Fe 3d valence bands. The origin of this enhancement is that the Fe 3d conduction bands energetically overlap with Bi 6p bands. Their results indicate the significance of spin-orbit coupling in Fe 3d conduction bands in relation to the large magneto-optical effect observed in BIG.

However, the results of recent GGA+U calculation by Li et al. [12] show that quite the contrary, Bi 6p orbitals in BIG hybridize significantly with Fe 3d orbitals in the lower conduction bands, leading to large V_{SO} -induced band splitting in the bands. Consequently, the transitions between the upper valence bands and lower conduction bands are greatly enhanced when Y is replaced by Bi. Such contradictions turn out to be typical for various "ab-initio" DFT based calculations.

E. Exchange-relativistic interaction and unconventional magneto-optics of weak ferromagnetic orthoferrites

Interestingly that circular magneto-optic effects in weak ferromagnets are anomalously large and are comparable with the effects in ferrite garnets despite two-three orders of magnitude smaller magnetization [3, 65, 68, 78–81]. In 1989 the anomaly has been assigned to a novel type of magneto-optical mechanisms related with exchange-relativistic interactions, in particular, with so-called spin-other-orbit coupling [54].

We have shown that an antisymmetric exchange-

relativistic spin-other-orbit coupling gives rise to an unconventional "antiferromagnetic" contribution to the circular magnetooptics for weak ferromagnets which can surpass conventional "ferromagnetic" term [25–29, 31, 54] (see, also Ref. [79]).

The gyration vector in weak ferromagnets is a sum of so-called ferromagnetic and antiferromagnetic terms with identical transformation properties, see Exp. (36). It should be noted that within the two-sublattice model for orthoferrites we neglect weak antiferromagnetic A- and C-modes (see, e.g., Refs. [56–58, 63]).

For the first time the antiferromagnetic contribution to circular MOE was experimentally identified and evaluated in orthoferrite YFeO₃ [54]. An analysis of the field dependence of the Faraday rotation $\Theta_F(\mathbf{H}_{ext})$ made it possible to determine all the contributions to the gyration vector ($\lambda = 0.6328 \mu\text{m}$):

$$A_{zz}m_z = (0.95 \pm 0.55) \cdot 10^{-3}; \quad B_{zx}|l_x| = (3.15 \pm 0.55) \cdot 10^{-3};$$

$$A_{xx}m_x = (0.2 \pm 0.7) \cdot 10^{-3}; \quad B_{xz}|l_z| = (-2.1 \pm 1.0) \cdot 10^{-3};$$

$$C_{zz} \approx C_{xx} = (-1.1 \pm 2.8) \cdot 10^{-6} kOe^{-1}, \quad (50)$$

where $|l_x| \approx |l_z| \approx 1$. Interestingly, rather large measurement errors allow for certain to determine only the fact of a large if not a dominant antisymmetric antiferromagnetic contribution related with antisymmetric spin-other-orbit coupling. Strictly speaking, the mutual orientation of the ferro- (\mathbf{m}) and antiferromagnetic (\mathbf{l}) vectors depends on the sign of the Dzyaloshinskii vector [56–58]. Interestingly, a rather arbitrarily chosen relative orientation of these vectors in Ref. [54] with positive sign of m_z and l_x exactly matches the theoretical predictions about the sign of the Dzyaloshinskii vector [56–58].

Existence of spontaneous spin-reorientational phase transitions $\Gamma_4(F_z G_x) \rightarrow \Gamma_2(F_x G_z)$ in several rare-earth orthoferrites does provide large opportunities to study anisotropy of circular magnetooptics [3, 27–29, 31, 65, 78]. Gan'shina *et al.* [28] measured the equatorial Kerr effect in EuFeO₃, TmFeO₃, and HoFeO₃ and have found the the gyration vector anisotropy in a wide spectral range 1.5–4.5 eV. The magneto-optical spectra, both real and imaginary parts of the gyration vector, were nicely fitted within a microscopic model theory based on the dominating contribution of the O2p–Fe3d charge transfer transitions and spin-other-orbit coupling in [FeO₆]⁹⁻ octahedra. An example of modeling the spectrum of the real part of the gyration vector in orthoferrite EuFeO₃ is shown in Figure 6. Let us again pay attention to the comparable values of circular MOEs in orthoferrites and ferrite garnets at more than an order of magnitude lower magnetic moment in weak ferromagnets of the YFeO₃ type and longitudinal ferrimagnets of the YIG type. The authors [28] have demonstrated a leading contribution of the antisymmetric spin-other-orbit coupling and estimated effective orbital magnetic fields in excited ⁶T_{1u} states of the [FeO₆]⁹⁻ octahedra, $H_L \sim 100 T$. These

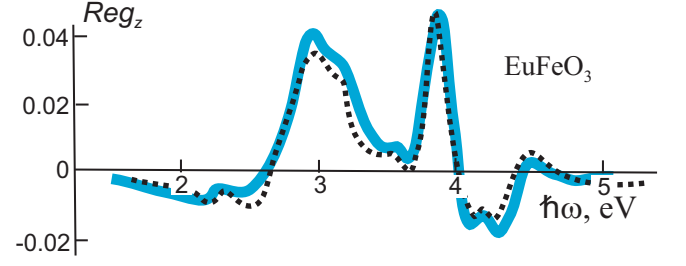


FIG. 6. Spectral dependence of the real part of the z-component of the gyration vector in EuFeO₃: experimental data are shown by dotted curve, model fitting is shown by solid curve.

anomalously large fields can be naturally explained to be a result of strong exchange interactions of the charge transfer ⁶T_{1u} states with nearby octahedra that are determined by a direct *p-d* exchange.

Whereas the existence of the antiferromagnetic contribution to the gyration vector is typical of a large number of multisublattice magnetic materials, the antisymmetry of the tensor \overleftrightarrow{B} is a specific feature of weak ferromagnets alone. In the case of rhombohedral weak ferromagnets such as FeBO₃, FeF₃, or α -Fe₂O₃, the tensor \overleftrightarrow{B} , governing the antiferromagnetic contribution to the Faraday effect is entirely due to the antisymmetric contribution, in view of the requirements imposed by the crystal symmetry. In crystals of this kind the appearance of the antiferromagnetic contribution to the gyration vector is entirely due to allowance for the antisymmetric spin-other-orbit coupling.

However, the data on the anisotropy of the Faraday effect in TmFeO₃ [78] and the values of the Faraday effect in SmFeO₃ ($\mathbf{m} \parallel a$ -axis) and a number of other orthoferrites with $\mathbf{m} \parallel c$ -axis [65] bear evidence of the existence of an appreciable symmetric AFM $\hat{B}^s \mathbf{l}$ contribution to the gyration vector of orthoferrites. Indeed, the Faraday effect in the Γ_4 phase ($\mathbf{m} \parallel c$) and in the Γ_2 phase ($\mathbf{m} \parallel a$) is determined, respectively, by the *z*- and *x*-component of \mathbf{g} :

$$g_z = A m_z + B_{zx} l_x; \quad g_x = A m_x + B_{xz} l_z \quad (51)$$

(under the justified assumption that \hat{A} be isotropic). Since $\mathbf{m} \perp \mathbf{l}$ and $m_x \approx m_z = m$, letting $l_x = 1$ with the view of the definitude, we obtain:

$$g_z = A m + B_{zx}^a + B_{zx}^s; \quad g_x = A m + B_{zx}^a - B_{zx}^s, \quad (52)$$

so that the experimentally found ratio [65, 78] $Re g_z / Re g_x \approx 2.5 - 3$ (at $\lambda \approx 1 - 2 \mu\text{m}$) indicates unambiguously the existence of an appreciable symmetric AFM term B_{zx}^s :

$$\frac{B_{zx}^s}{A m + B_{zx}^a} \sim 0.5.$$

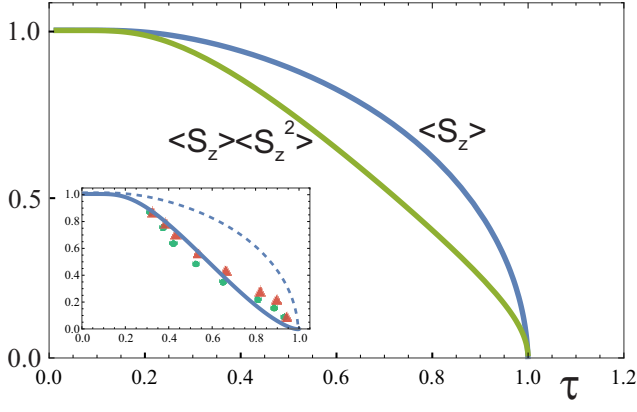


FIG. 7. Temperature dependence of the normalized thermodynamic quantities determining the temperature dependence of the circular MOE. The inset shows an example of fitting the experimental data on the temperature dependences of the equatorial Kerr effect in hematite $\alpha\text{-Fe}_2\text{O}_3$ (see Figure 6 in Ref. [68]) using the two-parameter formula (56), dotted curve is the $\langle S_z \rangle$ dependence.

F. The temperature dependence of the circular magneto-optics of ferrites

The analysis of the temperature dependences of *MOE* can yield an important information about the role of var-

ious mechanisms of the circular *MOE*. Experimental studies of the Faraday and Kerr effects in weak ferromagnets $\alpha\text{-Fe}_2\text{O}_3$ [79], FeBO_3 [80, 81], YFeO_3 [68] have shown that their circular *MOE* and the magnetic moment, both total and that of each sublattice, have *different* temperature dependences. In Refs. [68, 79, 81], an attempt was made to connect this phenomenon with the so-called *pair* transitions.

However, we show here that all peculiarities of the temperature dependence of the Faraday and Kerr effects for weak ferromagnets can be naturally and consistently explained by taking into account the *AFM* $\hat{B}\hat{I}$ contribution to the gyration vector due to the exchange-relativistic interactions. Whereas the *FM* $\hat{A}\hat{m}$ contribution to \mathbf{g} (36), the *AFM* $\hat{B}^{sym}\mathbf{1}$ contribution due to *LSCF* in ${}^6T_{1u}$ *CT* states (36), and the contributions due to intra-center V_{so}^{ex} have the temperature dependence determined by the ordinary thermodynamic average of the spin $\langle S(m) \rangle$, the *AFM* contribution owing to the "spin-other orbit" interaction is related to the average value of a complicated spin operator $\hat{S}(mn)$ (15). In the molecular field approximation the thermodynamic average of the nonlinear operator \mathbf{S}_{mn} in (15) can be written as follows [82]

$$\langle \hat{S}_q(mn) \rangle = \langle \hat{S}_z(n) \rangle C_q^1(\mathbf{S}(n)) + \gamma \langle \hat{V}_0^2(S(m)) \rangle_T \langle \hat{S}_z(n) \rangle \sum_{q_1, q_2} \begin{bmatrix} 2 & 1 & 1 \\ q_1 & q_2 & q \end{bmatrix} C_{q_1}^2(\mathbf{S}(m)) C_{q_2}^1(\mathbf{S}(n)), \quad (53)$$

where $C_{q_1}^2(\mathbf{S}(m))$, $C_{q_2}^1(\mathbf{S}(n))$ are spherical tensorial harmonics ($C_q^k = \sqrt{\frac{4\pi}{2k+1}} Y_{kq}$) as the functions of classical spin direction;

$$\langle S_z \rangle = S B_S(x),$$

where $B_S(x)$ is the Brillouin function

$$B_S(x) = \frac{2S+1}{2S} \coth \frac{2S+1}{2S} x - \frac{1}{2S} \coth \frac{1}{2S} x; \quad x = \frac{3S}{S+1} \frac{\sigma}{\tau}$$

($\sigma = S_z/S$ and τ being the reduced magnetic moment and temperature, respectively);

$$\langle \hat{V}_0^2(S) \rangle_T = 2 \left[\frac{(2S-2)!}{(2S+3)!} \right]^{1/2} \left(3 \langle \hat{S}_z^2 \rangle - S(S+1) \right) \quad (54)$$

where

$$\left(3 \langle \hat{S}_z^2 \rangle - S(S+1) \right) = \left(2S(S+1) - 3S \coth \frac{x}{2S} \cdot B_S(x) \right), \quad (55)$$

Thus, the temperature dependence of the gyration vector in the molecular field approximation is determined by the following two-parameter formula :

$$g(T) = a \langle S_z \rangle + a' \langle S_z \rangle \langle S_z^2 \rangle \approx A m + A' m^3, \quad (56)$$

with the frequency dependent coefficients a , b . Temperature dependence of the thermodynamic factors $\langle S_z \rangle$ and $\langle S_z \rangle \langle S_z^2 \rangle$ are presented in Figure 7, where the inset shows an example of fitting experimental data on the temperature dependences of the equatorial Kerr effect in hematite $\alpha\text{-Fe}_2\text{O}_3$ (see Figure 6 in Ref. [68]) using the two-parameter formula (56).

In other words, the *MOE* in weak ferromagnets will be characterized by a clear nonlinear dependence on the magnetic moment of sublattices, the presence of which is a direct indication of the contribution of exchange-relativistic interactions of the spin-other-orbit type. As expected, the nonlinear contribution, both in magnitude and in sign, will depend substantially on the frequency [68, 79–81].

It is worth noting that Exp. (53) provides a dependence of the exchange-relativistic contribution to the gyration vector on the mutual orientation of neighboring spins.

G. The high-energy optics and magneto-optics of ferrites

The availability of modern high-intensity synchrotron radiation has facilitated the refinement of conventional spectroscopy. This is especially true in the field of *MOE*, where the synchrotron radiation is a convenient tool of obtaining the spectra at high energies.

Kučera *et al.* [84] have obtained the reflectivity spectra of a number of iron and non-iron garnets and yttrium orthoferrite in the vacuum ultraviolet 5 to 30 eV range using synchrotron radiation as the light source. Contrary to the visible and near UV regions, all the spectra obtained are strikingly similar in this spectral range. Two broad bands sited at about 10 and 17 eV have been found in both garnet and orthoferrite reflectivity and optic absorption spectra. The 10 eV band was assigned to the CT transition from the oxygen 2p valence band to the yttrium 4d or 5s conduction states. The band centered near 17 eV was attributed to the "orbital-promotion" inter-configurational Fe 3d → Fe 4p transition. Despite the large peak values, the contribution of these transitions to the MOE of ferrites in the visible region, being structureless, is significantly inferior to the contribution of O 2p-Fe 3d CT transitions.

H. Rare-earth ions in ferrites

The simplest expression for the contribution of the dipole-allowed 4f-5d transition to the rare-earth ion polarizability tensor can be obtained by neglecting the splitting of the 4fⁿ-15d- configuration [85]

$$\alpha_q^k = (-1)^{1+k} 3\sqrt{2k+1} \frac{1}{\hbar} \begin{Bmatrix} 3 & 3 & k \\ 1 & 1 & 2 \end{Bmatrix} e^2 r_{fd}^2 F_k(\omega, \omega_{fd}) \langle \hat{U}_q^k(J) \rangle \quad (57)$$

where $\{\dots\}$ is the 6j-symbol [59], $r_{fd} = \langle 4f|r|5d \rangle$ is the radial integral, $\langle \hat{U}_q^k(J) \rangle$ is the thermodynamical average of the irreducible tensor $\hat{U}_q^k(J)$ with submatrix element $U_{SLJ;SL'J'}^{(k)}$ [59].

The components of the tensor α_q^1 , which determines the contribution of the rare-earth ion to the circular magneto-optics, can be written as follows

$$\boldsymbol{\alpha} = -\frac{1}{7\sqrt{2}} e^2 r_{fd}^2 F_1(\omega, \omega_{fd}) \frac{2-g_J}{g_J \mu_B} \mathbf{m}_R, \quad (58)$$

where \mathbf{m}_R is the magnetic moment of the R-ion, g_J is the Lande-factor. The symmetric anisotropic part of the polarizability tensor determines the effects of linear birefringence and dichroism. In Cartesian form, we get [85]

$$\alpha_{ij} = \frac{\sqrt{3}}{14} e^2 r_{fd}^2 F_2(\omega, \omega_{fd}) \alpha \langle 3\widetilde{J}_i \widetilde{J}_j - J(J+1) \rangle, \quad (59)$$

where $\widetilde{J}_i \widetilde{J}_j = \frac{1}{2}(\hat{J}_i \hat{J}_j + \hat{J}_j \hat{J}_i)$, α is the Stevens parameter [86].

A detailed analysis of the role of the effects of a strong crystal field for the 5d electron was carried out in Refs. [85, 87].

VII. CONCLUSIONS

The paper presents the theory of the optical and magneto-optical properties of strongly correlated iron oxides, primarily ferrite garnets and orthoferrites, based on the cluster model with the leading contribution of the charge transfer transitions.

At variance with the "first-principles" DFT based band models the cluster model is physically clear, it allows one to describe both impurity and dilute and concentrated systems, provides a self-consistent description of the optical, magnetic, and magneto-optical characteristics of Fe centers with a detailed account of local symmetry, low-symmetry crystal field effects, spin-orbit and Zeeman interactions, and also relatively new exchange-relativistic interaction, which plays a fundamental role for the circular magneto-optics of weak ferromagnets.

The cluster approach provides a regular procedure for classifying and estimating the probability of allowed and forbidden electric-dipole CT transitions and their contribution to optical and magneto-optical anisotropy.

The cluster model makes it possible to describe all the specific features of the influence of Bi ions on the circular magneto-optics of ferrites by the Bi 6p-O 2p hybridization and partial Bi-O "transfer" of the large Bi 6p spin-orbit interaction. The cluster model predicts the "selective" nature of the influence of Bi only on certain CT transitions, the appearance of an anisotropy of the ferromagnetic contribution, and the absence of any influence on the field contribution to the gyration vector.

The contribution of the exchange-relativistic interaction for the excited ${}^6T_{1u}$ terms in $[\text{FeO}_6]^{9-}$ clusters leads not only to the appearance of an "antiferromagnetic" contribution to the gyration vector of weak ferromagnets such as orthoferrite RFeO_3 and hematite $\alpha\text{-Fe}_2\text{O}_3$ but also to the deviation of the temperature dependence of circular MOE from the simple proportionality to the magnetization \mathbf{m} . The appearance of a nonlinear \mathbf{m} -dependence is an indication of the contribution of the unusual "spin-other-orbit" interaction in excited ${}^6T_{1u}$ states.

Undoubtedly, the considered version of the cluster theory requires more detailed development both in terms of improving the used MO-LCAO scheme and in terms of the possible application of the "hybrid" LDA + MLFT scheme [24]. In any case, development the cluster model of magneto-optical effects in ferrites needs data from systematic experimental studies of the concentration, spectral, and temperature dependences of various optical and magneto-optical effects for Fe centers in oxides.

ACKNOWLEDGMENTS

This study was supported by the Ministry of Science and Higher Education of the Russian Federation, project FEUZ-2023-0017

REFERENCES

-
- [1] Moskvina, A. S., Cluster theory of charge-transfer excitations in strongly correlated oxides. *Optics and Spectroscopy*, **111**, 403-410 (2011).
- [2] Moskvina, A. S., DFT, L(S)DA, LDA+U, LDA+DMFT, ..., whether we do approach to a proper description of optical response for strongly correlated systems?. *Optics and Spectroscopy*, **121** 467-477 (2016).
- [3] F. J. Kahn, P. S. Pershan, and J. P. Remeika, Ultraviolet Magneto-Optical Properties of Single-Crystal Ferrimagnetic Ferric Oxide Compounds, *Phys. Rev.* **186**, 891 (1969).
- [4] H. Hohenberg and W. Kohn, Inhomogeneous Electron Gas, *Phys. Rev.* **136**, B864 (1964).
- [5] W. Kohn and J. L. Sham, Self-Consistent Equations Including Exchange and Correlation Effects, *Phys. Rev.* **140**, A1133 (1965).
- [6] T. Oikawa, S. Suzuki, K. Nakao, First-Principles Study of Spin-Orbit Interactions in Bismuth Iron Garnet, *Journal of the Physical Society of Japan*, 2005, 74, 401-404
- [7] F. Iori, A. Teurtrie, L. Bocher, E. A. Popova, N. Keller, O. St'ephan, A. Gloter, Bismuth iron garnet: Ab initio study of electronic properties, *Physical Review B*, 2019, 100, 245150
- [8] Hiroki Nakashima, Abdul-Muizz Pradipto, Toru Akiyama, Tomonori Ito, Kohji Nakamura, Electron correlation effects and magneto-optical properties of yttrium iron garnet, *AIP Advances*, 2020, 10, 045029
- [9] V. I. Anisimov and Yu. A. Izyumov, *Electronic Structure of Strongly Correlated Materials* (Springer Verlag, Berlin, 2010).
- [10] W. Y. Ching, Z.-Q. Gu, and Y.-N. Xu, Theoretical calculation of the optical properties of Y₃Fe₅O₁₂, *J. Appl. Phys.* **89**, 6883 (2001).
- [11] L.-S. Xie, G.-X. Jin, L. He, G. E. W. Bauer, J. Barker, and K. Xia, First-principles study of exchange interactions of yttrium iron garnet, *Phys. Rev. B* **95**, 014423 (2017).
- [12] Wei-Kuo Li, G. Guo, First-principles study on magneto-optical effects in the ferromagnetic semiconductors Y₃Fe₅O₁₂ and Bi₃Fe₅O₁₂, *Phys. Rev. B* **103**, 014439 (2021).
- [13] Kun Xu, Luo Zhang, Andy Godfrey, Dongsheng Song, Wenlong Si, Yawen Zhao, Yi Liu, Yiheng Rao, Huaiwu Zhang, Heng-An Zhou, Wanjun Jiang, Wenbin Wang, Zhiying Cheng, and Jing Zhu, Atomic-scale insights into quantum-order parameters in bismuth-doped iron garnet, *PNAS* 2021 Vol. 118 No. 20 e2101106118
- [14] K. Burke, Perspective on density functional theory, *J. Chem. Phys.* **136**, 150901 (2012).
- [15] K. H. Ahn and A. J. Millis, Effects of magnetic ordering on the anisotropy and temperature dependence of the optical conductivity in LaMnO₃: A tight-binding approach, *Phys. Rev. B* **61**, 13545 (2000).
- [16] P. Ravindran, A. Kjekshus, H. Fjellvag, A. Delin, and O. Eriksson, Ground-state and excited-state properties of LaMnO₃ from full-potential calculations, *Phys. Rev. B* **65**, 064445 (2002).
- [17] E. S. Kryachko, E. V. Ludena, Density functional theory: Foundations reviewed, *Physics Reports* **544** (2014) 123239.
- [18] V. V. Mazurenko and V. I. Anisimov, Weak ferromagnetism in antiferromagnets: ??Fe₂O₃ and La₂CuO₄, *Phys. Rev. B* **71**, 184434 (2005); M. I. Katsnelson, Y. O. Kvashnin, V. V. Mazurenko, and A. I. Lichtenstein, Correlated band theory of spin and orbital contributions to Dzyaloshinskii-Moriya interactions, *Phys. Rev. B* **82**, 100403(R) (2010).
- [19] C. Roedel and F. Bechstedt, Optical and energy-loss spectra of the antiferromagnetic transition metal oxides MnO, FeO, CoO, and NiO including quasiparticle and excitonic effects, *Phys. Rev. B* **86**, 235122 (2012).
- [20] A. D. Becke, Perspective: Fifty years of density-functional theory in chemical physics, *J. Chem. Phys.* **140**, 18A301 (2014).
- [21] J. Ghijsen, L. H. Tjeng, J. van Elp, H. Eskes, J. Westerink, G. A. Sawatzky, and M. T. Czyzyk, Electronic structure of Cu₂O and CuO, *Phys. Rev. B* **38**, 11322 (1988).
- [22] H. Eskes, L.H. Tjeng, and G. A. Sawatzky, Cluster-model calculation of the electronic structure of CuO: A model material for the high-T_c superconductors, *Phys. Rev. B* **41**, 288 (1990).
- [23] S. Sugano, Y. Tanabe and H. Kamimura, *Multiplets of Transition-Metal Ions in Crystals* (Academic, New York, 1970).
- [24] M. W. Haverkort, M. Zwierzycki, and O. K. Andersen, Multiplet ligand-field theory using Wannier orbitals, *Phys. Rev. B* **85**, 165113 (2012).
- [25] Yu. P. Gaidukov, A. V. Zenkov, S. V. Koptsik, G. S. Krinchik, A. S. Moskvina, Nature of high magneto-optic activity of crystals with Fe³⁺ ions, *JETP Letters*, 1990, 51, 228-231
- [26] Moskvina, A. S. ; Zenkov, A. V. ; Yuryeva, E. I. ; Gubanov, V. A., Origin of the magneto-optical properties of iron garnets. *Physica B: Physics of Condensed Matter*. **168**, 187-196 (1991).
- [27] G. S. Krinchik, A. S. Moskvina, E. A. Ganshina, S. V. Koptsik, A. Yu. Trifonov, A. V. Zenkov, *Advances in Magneto-Optics II*, Proc. 2nd Int. Symp. Magneto-Optics, *Fizika Nizkih Temperatur*, **18**, Supplement, No..S1, 5 (1992).
- [28] E. A. Gan'shina, A. V. Zenkov, G. S. Krinchik, A. S. Moskvina, and A. Yu. Trifonov, *Fizika Tverdogo Tela*, **33**, 1122 (1991) (*Sov. Phys. Solid State* **33**, 637 (1991)).
- [29] E. A. Gan'shina, A. V. Zenkov, G. S. Krinchik, A. S. Moskvina, and M. M. Nishanova, *Fizika Tverdogo Tela*, **34**, 3319 (1992) [*Sov. Phys. Solid State* **34**, 1776 (1992)].
- [30] Moskvina, A. S. ; Zenkov, A. V., Huge magneto-optic ef-

- fects in Bi-containing iron garnets: A theoretical consideration. *Solid State Communications*. **80**, 739-741 (1991).
- [31] Moskvina, A. S. ; Zenkov, A. V. ; Ganshina, E. A. ; Krinchik, G. S. ; Nishanova, M. M., Anisotropy of the circular magneto-optics of orthoferrites: A theoretical consideration on the basis of the charge-transfer transitions and exchange-relativistic interactions concept. *Journal of Physics and Chemistry of Solids*. **54**, 101-105 (1993).
- [32] Zenkov, A. V. ; Moskvina, A. S., Bismuth-induced increase of the magneto-optical effects in iron garnets: A theoretical analysis. *Journal of Physics Condensed Matter*. **14**, 6957-6968 (2002).
- [33] Pisarev, R. V. ; Moskvina, A. S. ; Kalashnikova, A. M. ; Rasing, Th. H. M., Charge transfer transitions in multiferroic BiFeO₃ and related ferrite insulators. *Physical Review B - Condensed Matter and Materials Physics*. **79**, 235128 (2009).
- [34] Moskvina, A. S. ; Pisarev, R. V., Optical spectroscopy of charge transfer transitions in multiferroic manganites, ferrites, and related insulators. *Low Temperature Physics*. **36** 489-510 (2010).
- [35] Moskvina, A. S. ; Neudert, R. ; Knupfer, M. ; Fink, J. ; Hayn, R., Character of charge transfer excitons in Sr₂CuO₂Cl₂. *Physical Review B - Condensed Matter and Materials Physics*. **65**, 1805121-1805124 (2002).
- [36] Moskvina, A. S. ; Malek, J. ; Knupfer, M. ; Neudert, R. ; Fink, J. ; Hayn, R. ; Drechsler, S. L. ; Motoyama, N. ; Eisaki, H. ; Uchida, S., Evidence for two types of low-energy charge transfer excitations in Sr₂CuO₃. *Physical Review Letters*. 2003 ; 91, № 3. 037001/1-037001/4.
- [37] Knupfer, Martin ; Fink, Jorg ; Drechsler, S. L. ; Hayn, Roland ; Malek, J. ; Moskvina, A. S., Two types of charge transfer excitations in low dimensional cuprates: An electron energy-loss study. *Journal of Electron Spectroscopy and Related Phenomena*. 2004 ; 137-140, № SPEC. ISS. 469-473.
- [38] Pisarev, R. V. ; Pavlov, V. V. ; Kalashnikova, A. M. ; Moskvina, A. S., Near-band gap electronic structure of the tetragonal rare-earth cuprates R₂CuO₄ and the bismuth cuprate Bi₂CuO₄. *Physical Review B - Condensed Matter and Materials Physics*. **82**, 224502 (2010).
- [39] Moskvina, A. S., Optical properties of low-dimensional cuprates. *Optical Materials*. **90**. 244-251 (2019).
- [40] Moskvina, A. S., One-center charge transfer transitions in manganites. *Physical Review B - Condensed Matter and Materials Physics*. **65**, 2051131-2051139 (2002).
- [41] Moskvina, A. S. ; Makhnev, A. A. ; Nomerovannaya, L. V. ; Loshkareva, N. N. ; Balbashov, A. M., Interplay of p-d and d-d charge transfer transitions in rare-earth perovskite manganites. *Physical Review B - Condensed Matter and Materials Physics*. **82**, 035106 (2010).
- [42] Sokolov, V. I. ; Pustovarov, V. A. ; Churmanov, V. N. ; Ivanov, V. Yu. ; Gruzdev, N. B. ; Sokolov, P. S. ; Baranov, A. N. ; Moskvina, A. S., Unusual x-ray excited luminescence spectra of NiO suggest self-trapping of the d-d charge-transfer exciton. *Phys. Rev. B* **86**, 115128 (2012).
- [43] V I Sokolov, V A Pustovarov, V N Churmanov, V Yu Ivanov, A Ye Yermakov, M A Uimin, N B Gruzdev, P S Sokolov, A N Baranov and A S Moskvina, Low-energy charge transfer excitations in NiO, *IOP Conference Series: Materials Science and Engineering*, **38**, 012007, (2012).
- [44] Likhtenshtein, A. I. ; Moskvina, A. S. ; Gubanov, V. A., Fe-3+-center electron structure and exchange interaction in rare-earth orthoferrites, **24**, 3596 (1982) (*Soviet Phys. Solid State* **24**, 2049 (1982)).
- [45] C. N. R. Rao, B. Raveau, *Transition Metal Oxides*, VCH, 1995.
- [46] S. Wittekoek, T. J. A. Popma, J. M. Robertson, and P. F. Bongers, Magneto-optic spectra and the dielectric tensor elements of bismuth-substituted iron garnets at photon energies between 2.2-5.2 eV, *Phys. Rev. B* **12**, 2777 (1975).
- [47] K. Shinagawa, *Magneto-Optics*, ed. S. Sugano and N. Kojima (Springer, Berlin, 2000), chap.5, p.137.
- [48] N. N. Kovaleva, A. V. Boris, C. Bernhard, A. Kulakov, A. Pimenov, A. M. Balbashov, G. Khaliullin, and B. Keimer, Spin-Controlled Mott-Hubbard Bands in LaMnO₃ Probed by Optical Ellipsometry, *Phys. Rev. Lett.* **93**, 147204 (2004).
- [49] I. B. Bersuker, *Electronic Structure and Properties of Transition Metal Compounds: Introduction to Theory*, Second Edition, John Wiley and Sons: New York, 2010.
- [50] A. M. Clogston, Optical Faraday rotation in ferrimagnetic garnets, *J. Phys. Radium* **20**, 151 (1959).
- [51] G. B. Scott, D. E. Lacklison, and J. L. Page, Absorption spectra of Y₃Fe₅O₁₂ (YIG) and Y₃Ga₅O₁₂: Fe³⁺, *Phys. Rev. B* **10**, 971 (1974).
- [52] J. H. Jung, K. H. Kim, D. J. Eom, T. W. Noh, E. J. Choi, J. Yu, Y. S. Kwon, Y. Chung, Determination of electronic band structures of CaMnO₃ and LaMnO₃ using optical-conductivity analyses, *Phys. Rev. B* **55**, 15489 (1997); J. H. Jung, K. H. Kim, T. W. Noh, E. J. Choi, and J. Yu, Midgap states of La_{1-x}Ca_xMnO₃: Doping-dependent optical-conductivity studies, *Phys. Rev. B* **57**, R11043 (1998).
- [53] P. A. Usachev, R. V. Pisarev, A. M. Balbashov, A. V. Kimel, A. Kirilyuk, and T. Rasing, Optical properties of thulium orthoferrite TmFeO₃, *Phys. Sol. State* **47**, 2292 (2005).
- [54] A. V. Zenkov, B. B. Krichevtsov, A. S. Moskvina, K. M. Mukimov, R. V. Pisarev, and M. M. Ruvinshtein, Anisotropy of the Faraday effect in the weak ferromagnet YFeO₃, *Zh. Eksp. Teor. Fiz.* 96, 1397 (1989) [*JETP*, 69, 792 (1989)].
- [55] Dzialoshinskii, I. E. *Thermodynamic Theory of Weak Ferromagnetism in Antiferromagnetic Substances. Soviet Physics JETP* **1957**, 5, 1259.
- [56] Moskvina, A. S., Microscopic theory of Dzyaloshinskii-Moriya coupling and related exchange-relativistic effects. *Journal of Magnetism and Magnetic Materials*. **400**. 117-120 (2016).
- [57] Moskvina, A., Dzyaloshinskii-Moriya Coupling in 3d Insulators. *Condensed Matter*. **4**, 84 (2019).
- [58] Moskvina, A. S., Dzyaloshinskii Interaction and Exchange-Relativistic Effects in Orthoferrites. *Journal of Experimental and Theoretical Physics*. **132**, 517-547 (2021).
- [59] I. I. Sobelman, *Introduction to the Theory of Atomic Spectra*, Pergamon Press, Oxford 1973.
- [60] Moriya, T. Anisotropic Superexchange Interaction and Weak Ferromagnetism. *Phys. Rev.* **1960**, 120, 91.
- [61] L. D. Landau and E. M. Lifshitz, *Electrodynamics of Continuous Media*, Pergamon Press, London 1960.
- [62] E. U. Condon and G. H. Shortley, *Theory of Atomic Spectra*, Cambridge University Press, New York 1935.
- [63] Moskvina, A., Structure-property relationships for weak ferromagnetic perovskites. *Magnetochemistry*. **7**, 111

- (2021).
- [64] R. B. Clover, C. Wentworth, and S. S. Mroczkowski, Low birefringent orthoferrites for optical devices, *IEEE Trans. Magn.* **7**, 480 (1971).
- [65] W. J. Tabor, A. W. Anderson, and L. G. van Uitert, Visible and Infrared Faraday Rotation and Birefringence of Single-Crystal Rare-Earth Orthoferrites, *J. Appl. Phys.* **41** (7), 3018 (1970).
- [66] M. V. Chetkin, Yu. S. Didosyan, and A. I. Akhutkina, Faraday effect in yttrium and dysprosium orthoferrites, *Fiz. Tverd. Tela* **13**, 3414 (1971).
- [67] I. S. Jacobs, H. F. Burne, and L. M. Levinson, Field-Induced Spin Reorientation in YFeO_3 and YCrO_3 , *J. Appl. Phys.* **42**, 1631 (1971).
- [68] V. E. Zubov, G. S. Krinchik, and V. A. Lyskov, Magneto-optical properties of hematite, *Zh. eksper. teor. Fiz.* **81**, 1489 (1981).
- [69] I. S. Griffith, *The Irreducible Tensor Method for Molecular Symmetry Groups*, Englewood Cliffs, New Jersey, 1962.
- [70] Krinchik G. S., Chetkin M. V., Transparent ferromagnets, *Sov. Phys. Usp.* **12** 307–319 (1969).
- [71] J. F. Dillon, *jr.* in: *Scuola Internazionale di Fisica "Enrico Fermi"*. *Fisica dei Granati Magnetici*, ed. A. Paoletti, North-Holland Publ.Co., 1978 (p.379).
- [72] A. K. Zvezdin and V. A. Kotov, *Magneto-Optics of thin Films*, Nauka, Moscow 1988 (in Russian).
- [73] P. Hansen, K. Witter, and W. Tolksdorf, Magnetic and magneto-optic properties of lead- and bismuth-substituted yttrium iron garnet films, *Phys.Rev. B* **27**, 6608 (1983).
- [74] G. B. Scott, D. E. Lacklison, H. I. Ralph, and J. L. Page, Magnetic circular dichroism and Faraday rotation spectra of $\text{Y}_3\text{Fe}_5\text{O}_{12}$, *Phys.Rev. B* **12**, 2562 (1975).
- [75] N. F. Kharchenko, L. I. Bely, and O. P. Tutakina, *Fiz. tverd. Tela* **10**, 2819 (1968).
- [76] E. V. Berdennikova and R. V. Pisarev, *Sov. Phys. Solid State* **18**, 45 (1976)].
- [77] K. Shinagawa: *Magneto-Optics*, ed. S. Sugano and N. Kojima (Springer, Berlin, 2000), chap.5, p.137.
- [78] M. V. Chetkin, Yu. I. Shcherbakov, A. P. Volenko, L. D. Schevchuk, Anisotropy of linear magneto-optical effects in thulium orthoferrite, *Zh. Eksp. Teor. Fiz.* **67**, 1027 (1974) [*Sov. Phys. JETP* **40**, 509 (1974)].
- [79] V. E. Zubov, V. A. Lyskov, and G. S. Krinchik, Exciton-phonon and exchange interaction effects on magneto-optical activity of yttrium orthoferrite, *Fiz. tverd. Tela* **26**, 2335 (1984).
- [80] V. E. Zubov, Temperature dependence of the equatorial Kerr effect in FeBO_3 *Fizika Tverdogo Tela*, **34**, 2098 (1992).
- [81] I. S. Edelman, A. V. Malakhovskii, T. I. Vasileva, and V. N. Seleznev, *Fiz. Tverd. Tela* **14**, 2810 (1972) [*Sov. Phys. Solid State* **14**, 2442 (1973)].
- [82] H. B. Callen, *Green Function Theory of Ferromagnetism*, *Phys.Rev.*, 1963, V.130, P.890.
- [83] J. C. Suits, Faraday and Kerr effects in magnetic compounds, *IEEE Trans.Magn.* **8**, 95 (1972).
- [84] M. Kučera, V. N. Kolobanov, V. V. Mikhailin, P. A. Orekhanov, and V. N. Makhov, REFLECTION SPECTRA OF SOME GARNET AND ORTHOFERRITE SINGLE-CRYSTALS IN VACUUM ULTRAVIOLET, *phys.stat.sol. (b)* **157**, 745 (1990).
- [85] A. S. Moskvina, V. M. Pleshchev, The 4f-5d transitions and polarizability of rare earth ions, *Optics and Spectroscopy*, 1988 **64**(4):432-434
- [86] K. N. R. Taylor, M. I. Darby, *Physics of Rare Earth Solids* (Chapman and Hall Ltd, London, 1972)
- [87] A. S. Moskvina and V. M. Pleshchev, Role of the crystal field in the circular magneto-optics of rare-earth crystals and glasses, *Optics and Spectroscopy*, 1990; **69**, 353-355